Mon. Not. R. Astron. Soc. **348,** 1255–1274 (2004) doi:10.1111/j.1365-2966.2004.07444.x

Neutral hydrogen gas in interacting galaxies: the NGC 6221/6215 galaxy group

Bärbel Koribalski[1★] and John M. Dickey[2,1]

[1]*Australia Telescope National Facility, CSIRO, PO Box 76, Epping, NSW 1710, Australia*
[2]*University of Minnesota, Department of Astronomy, 116 Church Street, S.E., Minneapolis, MN 55455, USA*

Accepted 2003 November 18. Received 2003 November 11; in original form 2003 September 15

ABSTRACT

Neutral hydrogen observations of the spiral galaxies NGC 6221 and 6215 with the Australia Telescope Compact Array (ATCA) reveal a wide, two-stranded bridge of at least 3×10^8 $M_\odot$ which can be traced between the two galaxies over a projected distance of 100 kpc. The velocity gradient of the H I bridge provides a rough estimate for the time since the encounter of 500 Myr. For NGC 6221, the brightest and most massive galaxy of the group, we derive a dynamical mass of $M_{\rm tot} = 8 \times 10^{10}$ $M_\odot$, while its companion NGC 6215 has a mass of only $M_{\rm tot} \sim 2 \times 10^9$ $M_\odot$. Further, we find three low-surface-brightness dwarf galaxies (Dwarfs 1, 2 and 3) in the neighbourhood of NGC 6221/15 with H I masses of 3.3, 0.6 and 0.3×10^8 $M_\odot$, respectively. The smallest, previously uncatalogued galaxy, Dwarf 3, lies between NGC 6221 and 6215, and may have formed out of bridge material.

The brightest part of the H I bridge lies roughly halfway between the interacting galaxies, indicating that bridge gas close to NGC 6221 and 6215 may have fallen back to the galaxies. The asymmetric extensions to the H I envelope of NGC 6221 are likely to be reaccreted gas, still settling in. Also, the peculiar velocity field of NGC 6215 may be explained by accreted bridge material settling into a plane offset from the old disc.

Key words: galaxies: individual: NGC 6215 – galaxies: individual: NGC 6221 – galaxies: interactions.

1 INTRODUCTION

NGC 6221 and 6215 are a nearby pair of southern spiral galaxies (see Fig. 1). Their relative proximity, and the peculiar appearance of NGC 6221 in the optical, Hα and H I (see Pence & Blackman 1984) suggest they are interacting. Individually, both galaxies have been studied over a large range of wavelengths: e.g. CO (Harnett, Loiseau & Reuter 1990; Aalto et al. 1995), Hα (Durret & Bergeron 1987; Ryder & Dopita 1993; Vega Beltrán et al. 1998), X-rays (Levenson et al. 2001), deep *B*- and *H*-band images (Eskridge et al. 2002), as well as Two-Micron All Sky Survey (2MASS) *J*-, *H*- and *K*-band images (Jarrett et al. 2003). For stellar population studies of NGC 6221, see, for example, Cid Fernandes et al. (2003) and Bonatto et al. (1998). Here we present a detailed study of the neutral hydrogen (H I) gas distribution and kinematics in NGC 6221, 6215 and their surroundings. Preliminary results were reported by Koribalski (1996a,b).

The systemic velocities of NGC 6221 and 6215, $v_{\rm HI} = 1481 \pm 11$ and 1555 ± 7 km s^{-1} (Reif et al. 1982; see also Table 1), differ by less than 100 km s^{-1}. The galaxies are separated by 18.6 arcmin (about five times the optical diameter of NGC 6221). Adopting a distance of $D = 18$ Mpc ($H_0 = 75$ km s^{-1} Mpc^{-1}) for the NGC 6221/15 galaxy group (1 arcsec = 87 pc) results in a projected distance between the two main galaxies of ~100 kpc.

NGC 6221 (Fig. 2, top) is a barred spiral galaxy with an optical diameter of ~3.5 × 2.5 arcmin^2 (18 × 13 kpc^2) and a position angle (PA) of 5°. Large amounts of dust are visible in both spiral arms as well as along the bar. NGC 6215 (Fig. 2, bottom) is generally classified as a non-barred spiral galaxy and has a smaller optical diameter of ~2.1 × 1.8 arcmin^2 (11 × 9 kpc^2), $PA = 78°$. Both galaxies are moderately inclined with inclination angles of $i = 43°$ and 38°, respectively. Eskridge et al. (2002) give morphological classifications derived from deep *B*- and *H*-band images of NGC 6221 (SABcd, SBb) and NGC 6215 (Scd, SABbc), respectively. For a summary of the galaxy properties, see Table 1.

The bar in NGC 6221, which is clearly visible in optical and infrared images (Laustsen, Madsen & West 1987; Sandage & Bedke 1994), lies at a *PA* of 118° (Pence & Blackman 1984) and has a length of ~1 arcmin (5.2 kpc). Two spiral arms extend symmetrically from the ends of the bar for ~1 arcmin. Beyond this, the northern arm sharply turns (>90°) and continues for another ~2 arcmin toward the southeast. This peculiar extension of the northern spiral arm is relatively faint in the infrared images (see Fig. 2). The turning

★E-mail: Baerbel.Koribalski@csiro.au

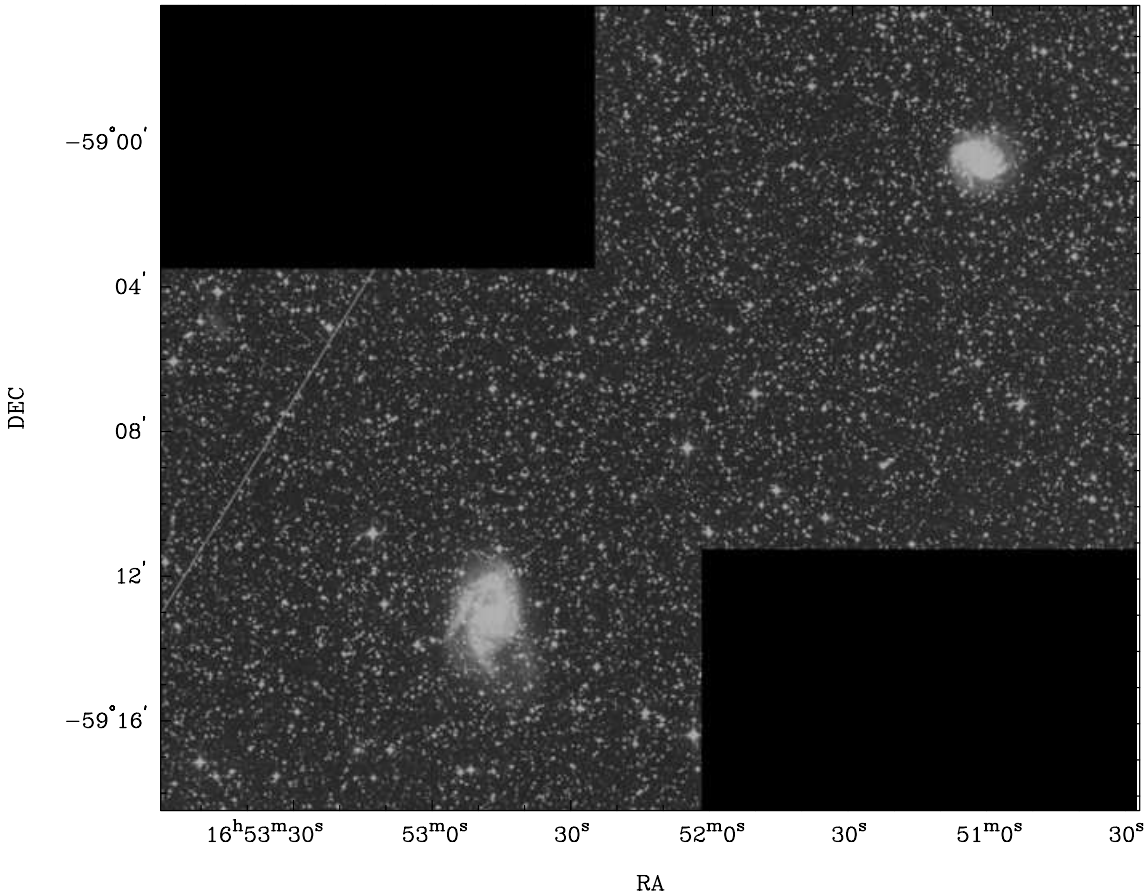

Figure 1. Optical UK Schmidt Telescope (UKST) *B*-band mosaic of the field containing the galaxies NGC 6221 (left) and 6215 (right), obtained from the Super COSMOS Sky Survey. The high density of stars in the foreground is due to the low Galactic latitude ($b \sim -10°$) of the galaxies. East is to the left and North to the top.

point (north of the nucleus) is marked by a blue H II region complex (Wray 1988) suggesting recent star formation, possibly induced by the interaction (see Section 3). In addition to this most peculiar, south-turning arm, there are another two southern extensions which are best seen in deep optical exposures (Pence & Blackman 1984): the southern spiral arm itself which seems to continue straight and, to the west of it, a faint stellar extension which has no obvious connection to the spiral arms. All three features together give NGC 6221 a triangular appearance in deep optical images, with the base toward the south. Ryder & Dopita (1993) point out that the southern arm may have split in two, with one part continuing on southward and the other part almost joining the northern arm as if trying to establish a ring. There appears to be a large amount of diffuse stellar emission surrounding the peculiar southern features.

Durret & Bergeron (1987) detect ionized gas from the nuclear region (approximately the inner 10 arcsec) as well as numerous H II regions along the spiral arms. The two brightest H II region complexes in the spiral arms, NE and N of the nuclear region, appear as blue star-forming regions in the colour image by Wray (1988). The nuclear spectrum of NGC 6221 is the superposition of an H II region-like spectrum and a very weak Seyfert 2 nucleus (Véron, Véron & Zuiderwijk 1981; Pence & Blackman 1984; Boisson & Durret 1986; Levenson et al. 2001). Cid Fernandes et al. (2003) give a mean starburst age of $10^{7.4\pm1.1}$ yr for the central 10×20 arcsec^2 of NGC 6221.

Kinematical studies of NGC 6221 using several long-slit spectra of the Hα line emission out to radii of 80 arcsec (Pence & Blackman 1984; Vega Beltrán et al. 1998) revealed very large non-circular motions of the ionized gas, possibly as a result of streaming motions along the bar and tidal interactions with NGC 6215. Recent Hα Fabry–Pérot observations of NGC 6221 and 6215 by Oddone et al. (1999) are promising, and we are looking forward to detailed velocity fields of the ionized gas.

NGC 6221 and 6215 have both been detected in CO(1–0). Using the 15-m Swedish–ESO Submillimetre Telescope (SEST), Harnett et al. (1990) obtained flux densities of $I_{\rm CO} = 20.0$ K km s^{-1} (NGC 6221) and 7.1 K km s^{-1} (NGC 6215) at their respective central positions. Aalto et al. (1995) measured slightly higher CO(1–0) flux densities of $I_{\rm CO} = 21.8 \pm 0.3$ K km s^{-1} (NGC 6221) and 8 ± 1 K km s^{-1} (NGC 6215). This corresponds to central molecular gas masses of $M_{\rm H_2} = 1.2 \times 10^9$ M$_\odot$ (NGC 6221) and 4.4×10^8 M$_\odot$ (NGC 6215) assuming a standard conversion factor of $N_{\rm H_2}/I_{\rm CO} = 2.3 \times 10^{20}$ H$_2$ cm^{-2} (K km s^{-1})$^{-1}$ (Strong et al. 1988).

The galaxy NGC 6300, which was suggested as a group member by Harnett et al. (1990), has a systemic velocity of $v_{\rm HI} = 1110 \pm 14$ km s^{-1} (Reif et al. 1982; Ryder et al. 1996) and lies SE of NGC 6221 at a projected distance of 278.5 arcmin ($\sim$1.5 Mpc). Its velocity and projected separation suggest that it is not part of the NGC 6221/15 group. The galaxies NGC 6215A ($v_{\rm sys} = 2740$ km s^{-1}) and ESO138–G001 ($v_{\rm sys} = 2894$ km s^{-1}) lie at projected distances of 11.0 and 16.2 arcmin, respectively, from NGC 6221. Their systemic velocities indicate that they are much more distant than NGC 6221 and not dynamically related.

Table 1. Some basic parameters of the observed spiral galaxies. References: (1) de Vaucouleurs et al. (1991), RC3; (2) Buta (1995); (3) Boisson & Durret (1986); (4) Reif et al. (1982); (5) Harnett et al. (1990); (6) Pence & Blackman (1984); (7) Aalto et al. (1995); (8) Sanders et al. (1995); (9) Jarrett et al. (2003).

	NGC 6221	NGC 6215	Ref.
Centre position:			
α(J2000)	$16^h52^m46^s.7$	$16^h51^m06^s.5$	(1)
δ(J2000)	$-59°12'59''$	$-58°59'36''$	
Type	.SBS5..	.SAS5..	(1)
	SB(s)bc p	SA(s)c p	(2)
Nuclear type	H II + Sy 2		(3)
Opt. diameter	$3'.5 \times 2'.5$	$2'.1 \times 1'.8$	(1)
Position angle	5°	78°	(1)
Inclination	43°	38°	(4)
Adopted distance (Mpc)	18	18	
Systemic velocities:			
$v_{\rm HI}$ (km s^{-1})	1481 ± 11	1555 ± 7	(4)
$v_{\rm CO}$ (km s^{-1})	1486 ± 4	1567 ± 4	(5)
$v_{\rm opt}$ (km s^{-1})	1350 ± 31	1521 ± 43	(1)
$v_{\rm H\alpha}$ (km s^{-1})	1475 ± 5	–	(6)
Integrated flux densities:			
$F_{\rm HI}$ (Jy km s^{-1})	76.0 ± 5.7	39.7 ± 4.4	(4)
$F_{\rm CO}$ (K km s^{-1})[a]	21.8 ± 0.3	8 ± 1	(7)
IRAS 60 μm (Jy)	49.13	30.83	(8)
IRAS 100 μm (Jy)	84.48	48.70	(8)
Optical photometry:			
B magnitude (mag)	11.04	11.64	(1)
$L_{\rm B}$ (10^9 L$_\odot$)	20.8	12.0	
2MASS total photometry:			
J band (mag)	8.104 ± 0.023	9.213 ± 0.024	(9)
H band (mag)	7.357 ± 0.024	8.499 ± 0.027	(9)
K band (mag)	7.121 ± 0.029	8.282 ± 0.034	(9)
3σ radius (arcsec)	81.19	45.6	(9)

[a]CO flux density measured in central pointing only.

Levenson et al. (2001) obtained *ASCA* X-ray data of the region, detecting NGC 6221 and 6215, the background galaxy ESO138–G001 (NGC 6215A is incorrectly identified), as well as a distant cluster[1] south of NGC 6221. They measure an X-ray luminosity of several times 10^{41} erg s^{-1} for NGC 6221, most of which comes from the central active galactic nucleus (AGN). Only a small amount of the X-ray emission appears to be thermal. NGC 6215 was detected at the extreme edge of the observed field. The archival *ROSAT* HRI image (see Fig. 3) shows three point sources around NGC 6221 that can also be identified in the *ASCA* image. The X-ray emission of NGC 6221 is clearly extended, but better data are needed to search for hot intragroup gas.

The paper is organized as follows. In Section 2 we summarize the observations and data reduction. In Section 3 we present the 20-cm radio continuum results and derive star formation rates (SFRs) for NGC 6221 and 6215. The H I morphology and kinematics of all members of the NGC 6221/15 galaxy group are described in Sections 4 and 5, respectively. The overall gas dynamics are discussed in Section 6, and Section 7 contains our conclusions.

[1] We find that the X-ray peak of the cluster 1RXS J165259.4–594302, as obtained from an archival *ROSAT* High Resolution Imager (HRI) image after smoothing, coincides with the galaxy WKK 7657 while a secondary peak can be associated with the galaxies WKK 7659 and WKK 7660. The galaxy redshifts are $z = 0.046$–0.049 (Di Nella et al. 1997; Woudt, Kraan-Korteweg & Fairall 1999). The north–south extent of the X-ray cluster is at least 20 arcmin (∼1 Mpc).

2 OBSERVATION AND DATA REDUCTION

The neighbouring galaxies NGC 6221 and 6215 were observed with the Australia Telescope Compact Array (ATCA) in 1995 March and August. H I line (IF 1) and wide-band 20-cm radio continuum (IF 2) data were obtained simultaneously using two ∼12-h observations each with the 1.5A and 375 arrays. For details of the observations, see Table 2. (The wide-band radio continuum data from IF 2 are not discussed in this paper.)

Data reduction was carried out with the AIPS and MIRIAD software packages using standard procedures. The narrow-band 20-cm data (IF 1) were split into a radio continuum and an H I line data set using a first-order fit to the line-free channels. The H I channel maps for each of the two pointings were made using 'natural' weighting of the *uv*-data in the velocity range from 1250 to 1750 km s^{-1} using steps of 10 km s^{-1}. The resulting synthesized beam is ∼32 arcsec; the measured rms is 1.4 mJy beam^{-1}.

Both H I data cubes were restored with circular beams of 35 arcsec and then corrected for primary beam attenuation using a taper to achieve approximately uniform noise across the image. This avoids excessive noise amplification at the edges of the primary beams. The rms in the overlap region between NGC 6221 and 6215 is ∼1 mJy beam^{-1}. One Jy beam^{-1} km s^{-1} corresponds to an H I column density of 0.9×10^{21} atoms cm^{-2}.

The H I moment maps were produced with the AIPS task MOMNT using Hanning smoothing over three channels (30 km s^{-1}) and a flux density cut-off of 2 mJy beam^{-1}.

Radio continuum maps were made using 'natural' and 'uniform' weighting of the narrow-band *uv*-data. After CLEANing they were restored with synthesized beams of 35 and 10 arcsec, respectively, resulting in an rms of 0.3 and 0.2 mJy beam^{-1}.

3 RADIO CONTINUUM RESULTS

Fig. 3 shows the overall distribution of the 20-cm radio continuum emission in the field toward the NGC 6221/15 galaxy group. Numerous background radio sources were detected, including the galaxy ESO138–G001. We detected extended continuum emission from both NGC 6221 and 6215 and measured flux densities of 334 and 282 mJy, respectively. No continuum emission was detected from the newly catalogued dwarf galaxies in the group (see Section 4), with upper limits to their flux densities of ∼1 mJy (5σ) assuming a point-source distribution.

Fig. 4 (top) shows the high-resolution continuum images of both galaxies. The radio core of NGC 6221 lies at the position α, δ(J2000) = $16^h52^m46^s.3$, $-59°13'01''$, in agreement with the optical, infrared and X-ray nucleus, and has a flux density of ∼54 mJy, a small fraction of the overall continuum emission from this galaxy. In Fig. 4 (bottom) we show the radial distribution of the radio continuum emission (per 2-arcsec rings, as well as accumulated flux density). We find a maximum flux density of 334 mJy out to a radius of ∼130 arcsec. The radio continuum emission in the extended disc is asymmetric, with a nearly vertical, ridge feature ∼20 arcsec to the east of the radio core indicating enhanced star formation activity in that part of the galaxy. In Fig. 5 we compare the radio continuum emission in the inner disc of NGC 6221 with the ionized gas distribution shown in the *Hubble Space Telescope* (*HST*) Wide Field Planetary Camera 2 (WFPC-2) image. The northern part of the ridge coincides with an extended, very bright H II region complex, which is also prominent in the Hα+[N II] image by Vega Beltrán et al. (1998). Its peculiar location (it is neither part of the bar nor the relatively symmetric spiral arms of NGC 6221) gives

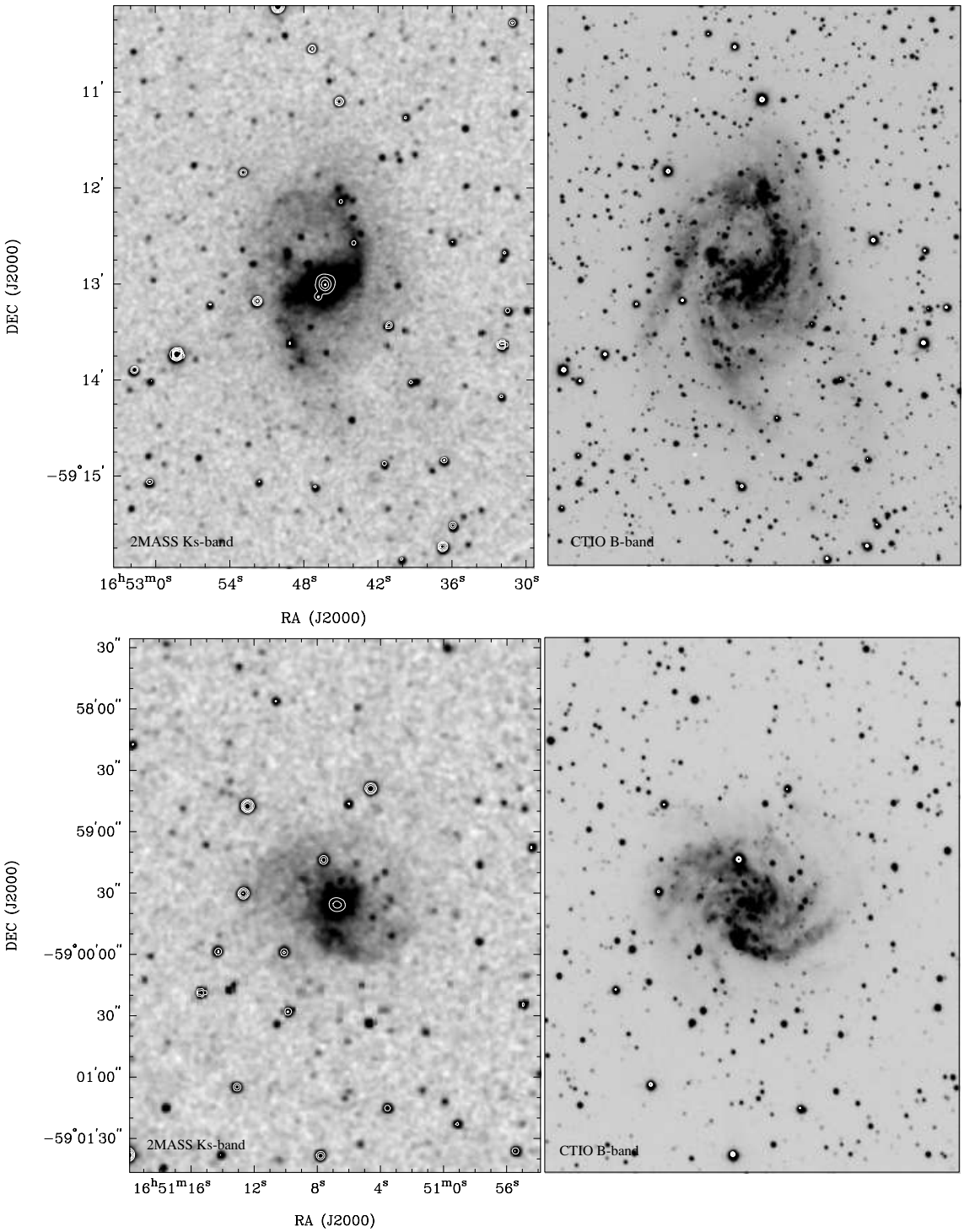

Figure 2. Infrared *Ks*-band images (left) and deep optical *B*-band images (right) of the two main galaxies, NGC 6221 (top) and 6215 (bottom), in the group. The infrared *Ks*-band images were obtained from 2MASS (Jarrett et al. 2003). The overlaid contours emphasize the bright infrared nuclei of the galaxies which coincide with their optical centre position. The deep optical *B*-band images were obtained by Eskridge et al. (2002) with the Cerro Tololo Inter-American Observatory (CTIO); the brightest stars are marked with contours. Similar deep optical images are available from Sandage & Bedke (1994). Most remarkable is the irregular dust pattern in the central region and the spiral arms of NGC 6221. Deep *H*-band images are also available from Eskridge et al. (2002).

the impression of an infalling dwarf galaxy. On the other hand, the position–velocity diagram taken across this H II region complex by Vega Beltrán et al. shows no peculiarities, indicating that it is most likely part of the regular rotation of NGC 6221. The position and size of the H II region complex are approximately α, δ (J2000) = $16^{\rm h}52^{\rm m}50^{\rm s}$, $-59^{\circ}12'40''$ ($\sim$30 arcsec northeast of the nucleus) and 5×10 arcsec^2. The middle of the ridge appears to be associated with the eastern end of the bar, and the southern end overlaps with numerous small H II regions in the southern spiral arm of NGC 6221. The northern spiral arm, only a small part of which is covered by

Table 2. Observing parameters.

ATCA configuration	1.5A	375
Date	25.3.1995	10.8.1995
Primary beam	33 arcmin	
Pointing positions in α, δ(J2000):		
NGC 6221	$16^{h}52^{m}45\overset{s}{.}71$	
	$-59^{\circ}13'29\overset{''}{.}05$	
Total observing time	724 min	592 min
NGC 6215	$16^{h}50^{m}49\overset{s}{.}42$	
	$-58^{\circ}59'7\overset{''}{.}09$	
Total observing time	671 min	792 min
IF 1:		
Centre frequency	1413 MHz	
Total bandwidth	8 MHz	
Number of channels	512	
Velocity resolution (after Hanning smoothing)	6.6 km s^{-1}	
Calibrator flux densities:		
Primary	1934–638 (14.88 Jy)	
Secondary	1718–649 (3.51 Jy)	
	1657–56 (1.45 Jy)	

the *HST* image (Fig. 5; see also Vega Beltrán et al. 1998), shows comparatively little radio continuum emission.

The radio core of NGC 6215 lies at the position α, δ(J2000) = $16^{h}51^{m}06\overset{s}{.}7$, $-58^{\circ}59'35''$, in agreement with the optical and infrared nucleus, and has a flux density of ∼18 mJy, again just a small fraction of the overall continuum emission. We find a maximum flux density of 282 mJy out to a radius of ∼110 arcsec. Similar to the ridge-like emission observed east of the NGC 6221 core, NGC 6215 shows enhanced continuum emission south-east of the core.

3.1 Star formation rates, efficiencies and ages

To estimate the SFRs of NGC 6221 and 6215 from their 20-cm radio continuum flux densities we use SFR (M$_{\odot}$ yr^{-1}) = 0.14 D^2 $F_{20\,\mathrm{cm}}$ derived from Condon (1992) and Haarsma et al. (2000), where D is the distance in Mpc and $F_{20\,\mathrm{cm}}$ is the 20-cm radio continuum flux density in Jy. For NGC 6221 and 6215 (D = 18 Mpc) we measure 334 and 282 mJy and hence overall SFRs of 15 and 13 M$_{\odot}$ yr^{-1}, respectively. Note that both galaxy cores contain only a small fraction of the total radio continuum flux density. In Fig. 4 we show the radial distribution of the radio continuum flux densities in NGC 6221 and 6215. This enables us to compare the radio derived SFR at any radius with that derived at other frequencies. For the three dwarf galaxies in the group we estimate SFR <0.1 M$_{\odot}$ yr^{-1}.

According to Levenson et al. (2001) the Hα luminosity from the nucleus of NGC 6221 (1.5 × 1.5 arcsec^2) corresponds to a SFR of 0.2 M$_{\odot}$ yr^{-1}. Storchi-Bergmann et al. (1994) report a much higher SFR of 5.9 M$_{\odot}$ yr^{-1} (adjusted to H_0 = 75 km s^{-1} Mpc^{-1}) in the central 10 × 20 arcsec^2 area, compared to the radio derived SFR of 5 M$_{\odot}$ yr^{-1} within a radius of 20 arcsec.

The SFR of a galaxy can also be estimated from its far-infrared (FIR) luminosity, L_{FIR}, using SFR (M$_{\odot}$ yr^{-1}) = 0.17 L_{FIR} (Kennicutt 1998), with L_{FIR} in units of 10^9 L$_{\odot}$. Using the *IRAS* 60- and 100-μm flux densities (see Table 1) we derive infrared luminosities of 2.7 × 10^{10} L$_{\odot}$ (NGC 6221) and 1.7 × 10^{10} L$_{\odot}$ (NGC 6215) which

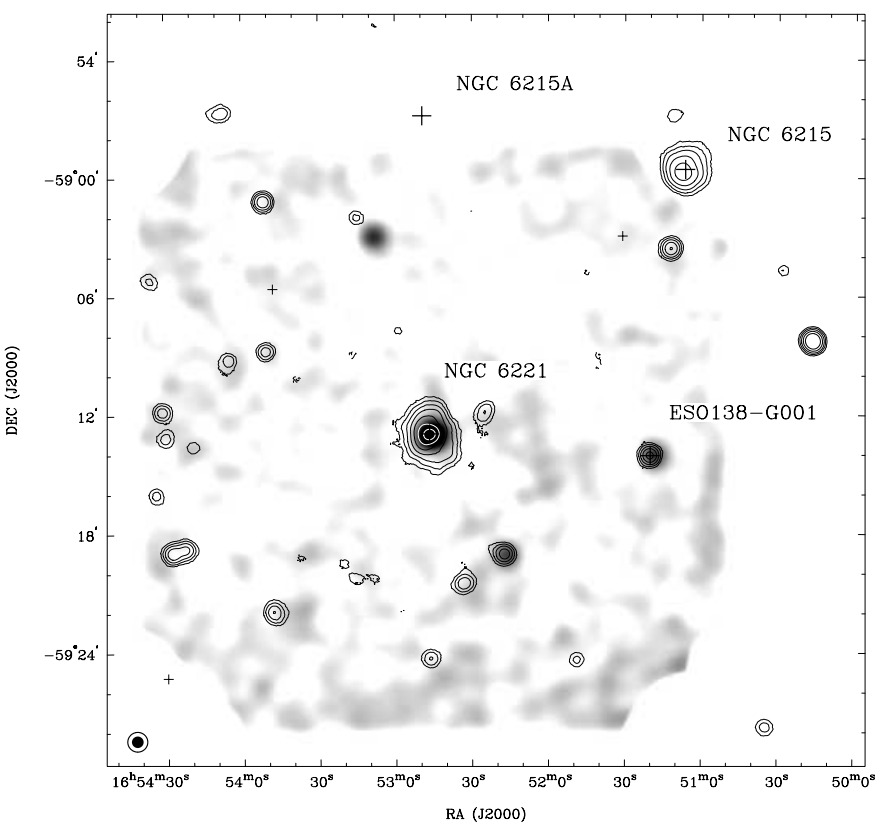

Figure 3. Low-resolution image of the 20-cm radio continuum emission (contours; 35 arcsec) toward the NGC 6221/15 galaxy group overlaid on to an archival *ROSAT* HRI X-ray image (grey-scale, convolved to 60-arcsec resolution). The contour levels are ±1.2, 2.5, 5, 10, 20, 40 and 80 mJy beam^{-1}. The group members as well as the background galaxies, NGC 6215A and ESO138–G001, are marked with crosses. The three dwarf galaxies, which were not detected in the radio continuum, are marked but not labelled.

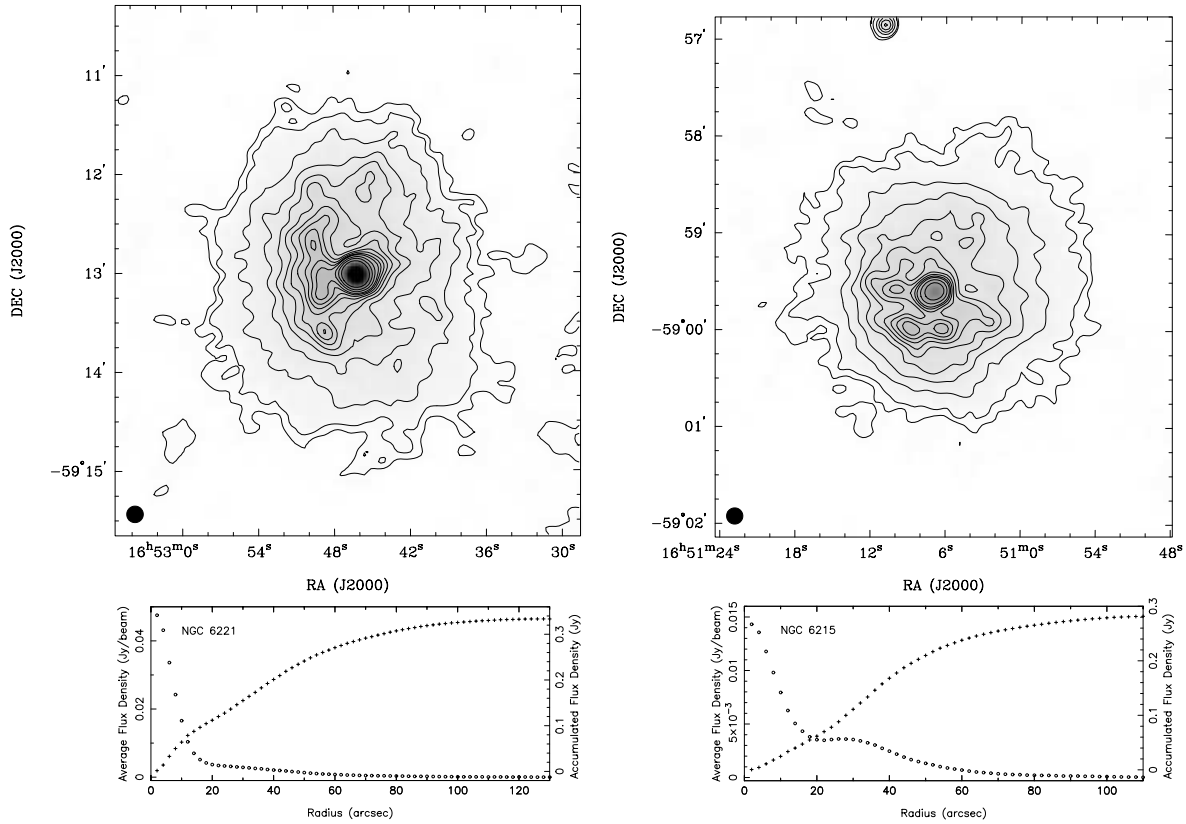

Figure 4. Top: High-resolution 20-cm radio continuum emission from NGC 6221 (left) and 6215 (right). The contour levels are 0.6 (3σ), 1, 2, 3, 4, 5, 6, 7, 8, 9, 10, 12, 15 and 20 mJy beam^{-1}. The synthesized beam (10 arcsec) is displayed at the bottom-left corner. Bottom: Radial distribution of the radio continuum emission from NGC 6221 (left) and 6215 (right). The average flux density per radius (in steps of 2 arcsec) is marked with circles and the accumulated flux density with crosses.

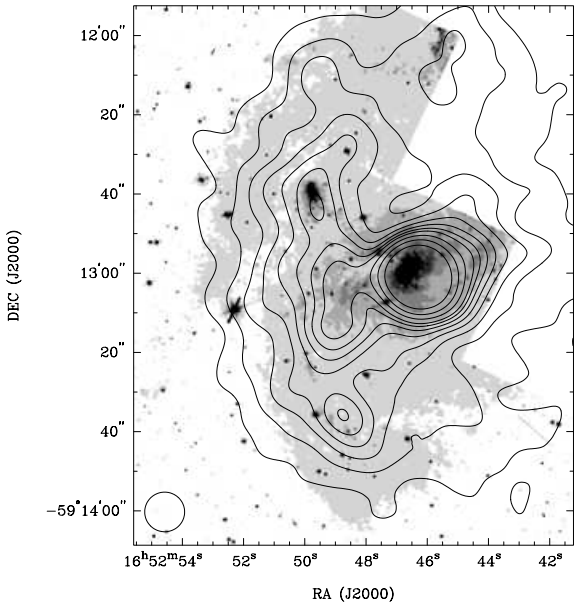

Figure 5. Radio continuum emission (contours) of the galaxy NGC 6221 overlaid on to an *HST* WFPC-2 image (grey-scale). The contour levels are 3, 4, 5, 6, 7, 8, 9, 10, 12, 15 and 20 mJy beam^{-1}. The beam (10 arcsec, see also Fig. 4) is displayed at the bottom-left corner. The WFPC-2 image (exposure = 500 s, pixel size = 0.2 arcsec) was obtained from the *HST* archive (see also Malkan et al. 1998). For this overlay the *HST* image was rotated and the coordinates adjusted to the optical centre.

correspond to SFRs of 4.6 and 2.9 $M_\odot$ yr^{-1}, respectively. Following Helou, Soifer & Rowan-Robinson (1985) we estimate the parameter q – the logarithm of the FIR to 1.4-GHz radio flux density ratio – as 2.3 (for NGC 6221) and 2.2 (for NGC 6215), compared to the average of $q \approx 2.3$ for normal spirals. In their models, Bressan, Silva & Granato (2002) find the lowest q values during the post-starburst phase. Thus, the difference between the radio and FIR emission (the radio emission fades more rapidly than the FIR emission after a starburst) can be used to study the star formation history of a galaxy.

Cid Fernandes et al. (2003) find the nuclear region (10 × 20 arcsec^2) of NGC 6221 dominated by an old (10^9–10^{10} yr) stellar population. While there is a significant intermediate (10^8 yr) population, little recent (10^6 yr) star formation is found. Their derived percentages of the total flux (at $\lambda_0 = 4020$ Å) for each age bin are 24 ± 9 (10^{10} yr), 24 ± 8 (10^9 yr), 26 ± 8 (10^8 yr), 19 ± 7 (10^7 yr) and 6 ± 5 (10^6 yr). They give a mean starburst age of $10^{7.4\pm1.1}$ yr for the central 10 × 20 arcsec^2 of NGC 6221.

We can only derive upper limits to the star formation efficiencies, SFE $= L_{\rm FIR}/M_{\rm H_2} \lesssim 23$ and 38 $M_\odot/L_\odot$, respectively, as the molecular gas content was measured within the central 43 arcsec of each galaxy whereas the FIR luminosity comes from a larger region (∼100 arcsec).

4 H I MORPHOLOGY

Fig. 6 shows the H I emission detected in the mosaic obtained by combining the pointings on NGC 6221 and 6215. Large amounts

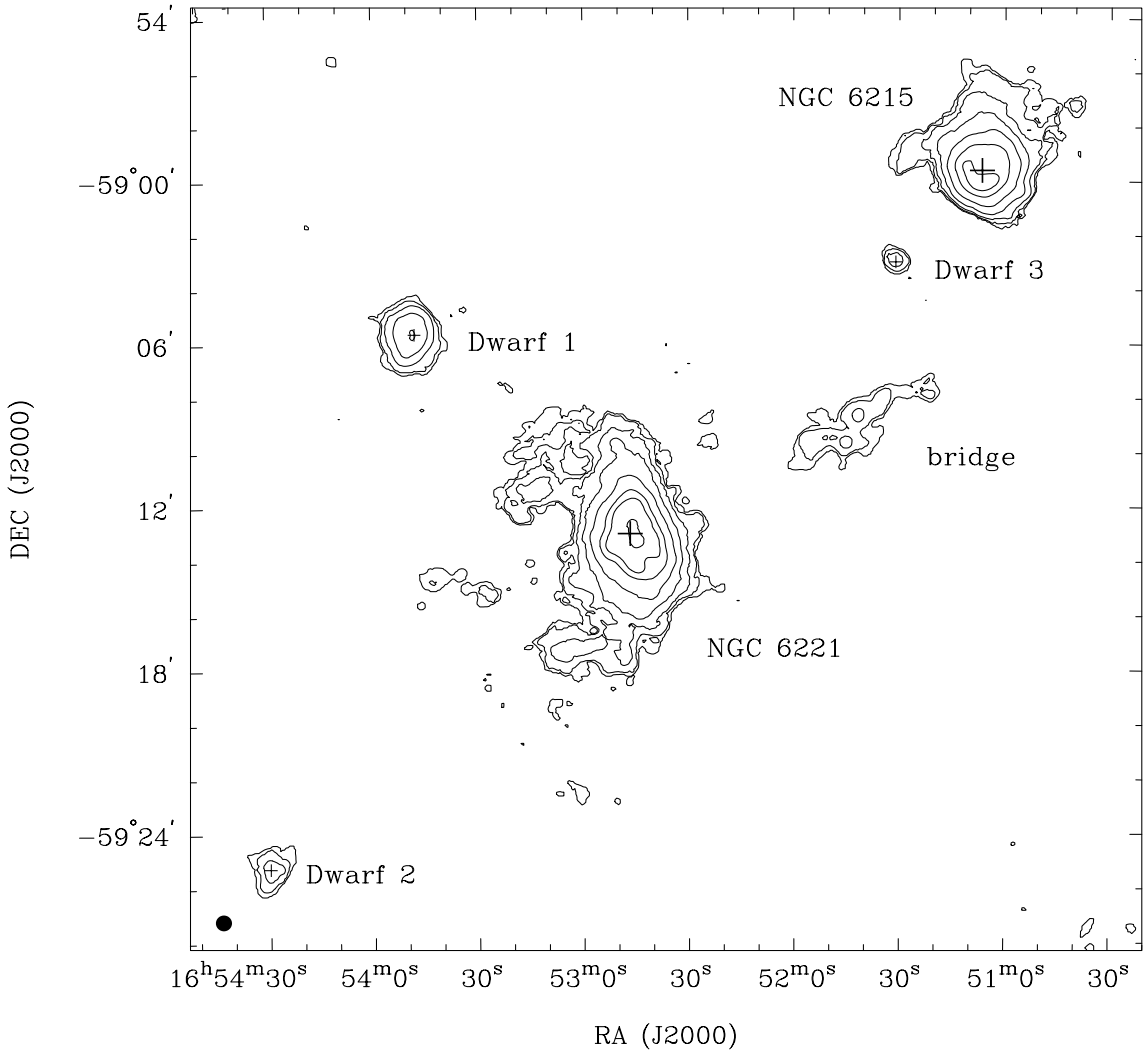

Figure 6. H I distribution in the NGC 6221/15 galaxy group. The contour levels are 0.05, 0.1, 0.2, 0.4, 0.8 and 1.6 Jy beam^{-1} km s^{-1}. The synthesized beam (35 arcsec) is displayed at the bottom-left corner. Crosses mark the galaxy centre positions. The brightest part of the H I bridge is located roughly mid-way between NGC 6221 and its companion, NGC 6215. The three dwarf galaxies are newly discovered members of this interacting group.

Table 3. H I properties of the galaxies and the bridge in the NGC 6221/15 group as measured with the ATCA.

Object	Proj. distance (arcmin)	Velocity range (km s^{-1})	$F_{\rm HI}$ (Jy km s^{-1})	$M_{\rm HI}$ (M$_\odot$)
NGC 6221	–	1310–1670	67.5	5.2×10^9
NGC 6215	18.6	1450–1660	35.2	2.7×10^9
Dwarf 1	11.1	1620–1690	4.3	3.3×10^8
Dwarf 2	17.9	1500–1550	0.8	6.1×10^7
Dwarf 3	14.0	1560–1630	0.4	2.7×10^7
Bridge	9.2	1460–1550	3.8	2.9×10^8

of extended H I gas are associated with the two spiral galaxies. In addition, we detect an elongated H I bridge between NGC 6221 and 6215 as well as H I emission from three low-surface-brightness dwarf galaxies. For summaries of the measured H I properties of all group components, see Tables 3 and 4. The H I bridge, peculiar extensions to the outer gas envelopes of NGC 6221 and 6215, and the southern optical extensions of NGC 6221 are all signs of galaxy interactions.

Fig. 7 shows the H I channel maps of the NGC 6221/15 group, excluding only the southernmost dwarf galaxy (Dwarf 2) which lies 18 arcmin southeast of NGC 6221. To show the overall distribution

Table 4. H I and optical properties of the dwarf galaxies in the NGC 6221/15 group. Note that for the H I diameters we quote the deconvolved Gaussian FWHM.

	Centre position, α, δ(J2000)		diameter (major × minor axis, *PA*)	
Object	H I	Optical	H I	Optical[a]
Dwarf 1	$16^{\rm h}53^{\rm m}48^{\rm s}.9$, $-59°05'36''.8$	$16^{\rm h}53^{\rm m}48^{\rm s}.5$, $-59°05'25''$	62 × 41 arcsec^2, 175°	74 × 42 arcsec^2, 225°
Dwarf 2	$16^{\rm h}54^{\rm m}29^{\rm s}.5$, $-59°25'16''.5$	$16^{\rm h}54^{\rm m}29^{\rm s}.7$, $-59°25'13''$	34 × 23 arcsec^2, 167°	52 × 15 arcsec^2, 145°
Dwarf 3	$16^{\rm h}51^{\rm m}31^{\rm s}.1$, $-59°02'54''.5$	$16^{\rm h}51^{\rm m}30^{\rm s}.6$, $-59°02'49''$	<35 arcsec, (229°)	20 × 15 arcsec^2, (240°)

[a]Estimates from Woudt & Kraan-Korteweg (2001) and Kraan-Korteweg (private communication).

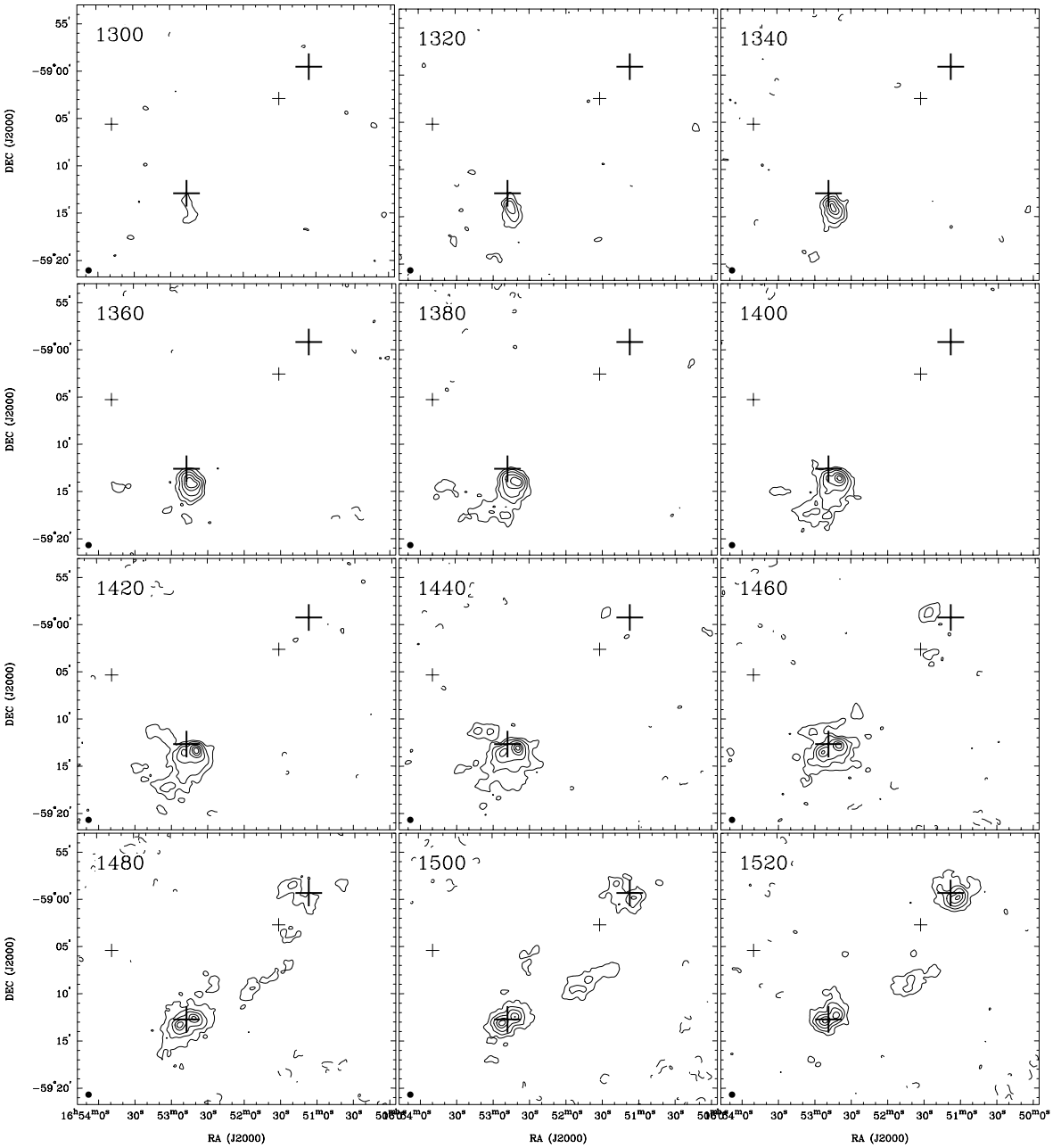

Figure 7. H I channel maps of the NGC 6221/15 group; the southernmost dwarf galaxy (Dwarf 2) lies outside the displayed field. The contour levels are ±2 (∼3σ), 4, 8, 16, 24, 32 and 40 mJy beam^{-1}. For this figure the H I channels were smoothed to a velocity resolution of 30 km s^{-1} and displayed in steps of 20 km s^{-1}. The synthesized beam (35 arcsec) is displayed in the bottom-left corner. The galaxy centre positions are marked with crosses.

and kinematics of the various components in the group, we smooth the H I channels to a velocity resolution of 30 km s^{-1}. The H I spectra of the main galaxies, NGC 6221 and 6215, as well as the three dwarf galaxies are displayed in Fig. 8. The most remarkable feature in the group is the H I bridge between NGC 6221 and 6215, which consists of two streams extending over a velocity range from ∼1460 to 1550 km s^{-1}; for further discussion, see Section 4.4. The H I spectrum of the bridge is displayed in Fig. 9.

Using the H I Parkes All Sky Survey (HIPASS; see, for example, Barnes et al. 2001) we measure $F_{\rm HI} = 154 \pm 18$ Jy km s^{-1} for the NGC 6221/15 group (resulting in $M_{\rm HI} = 1.2 \times 10^{10}$ M$_\odot$), while the ATCA measures only 112 ± 4 Jy km s^{-1} (∼70 per cent). It follows that ∼30 per cent or 3 × 10^9 M$_\odot$ of diffuse extended H I emission were not 'seen' by the interferometer. By jointly fitting two point sources to the HIPASS data of the group, we find $F_{\rm HI} = 91 \pm 7$ Jy km s^{-1} for NGC 6221 and $F_{\rm HI} = 57 \pm 7$ Jy km s^{-1} for NGC 6215. These values agree very well with those quoted in the HIPASS Bright Galaxy Catalogue (Koribalski et al. 2003).

4.1 The galaxy NGC 6221

Fig. 10 shows the H I distribution of NGC 6221, the mean H I velocity field and the H I velocity dispersion. The H I distribution shows a depression in the central region (see Fig. 13), possibly due to H I absorption against the radio continuum emission. The H I emission in NGC 6221 covers a velocity range from about 1310 to 1670 km s^{-1}.

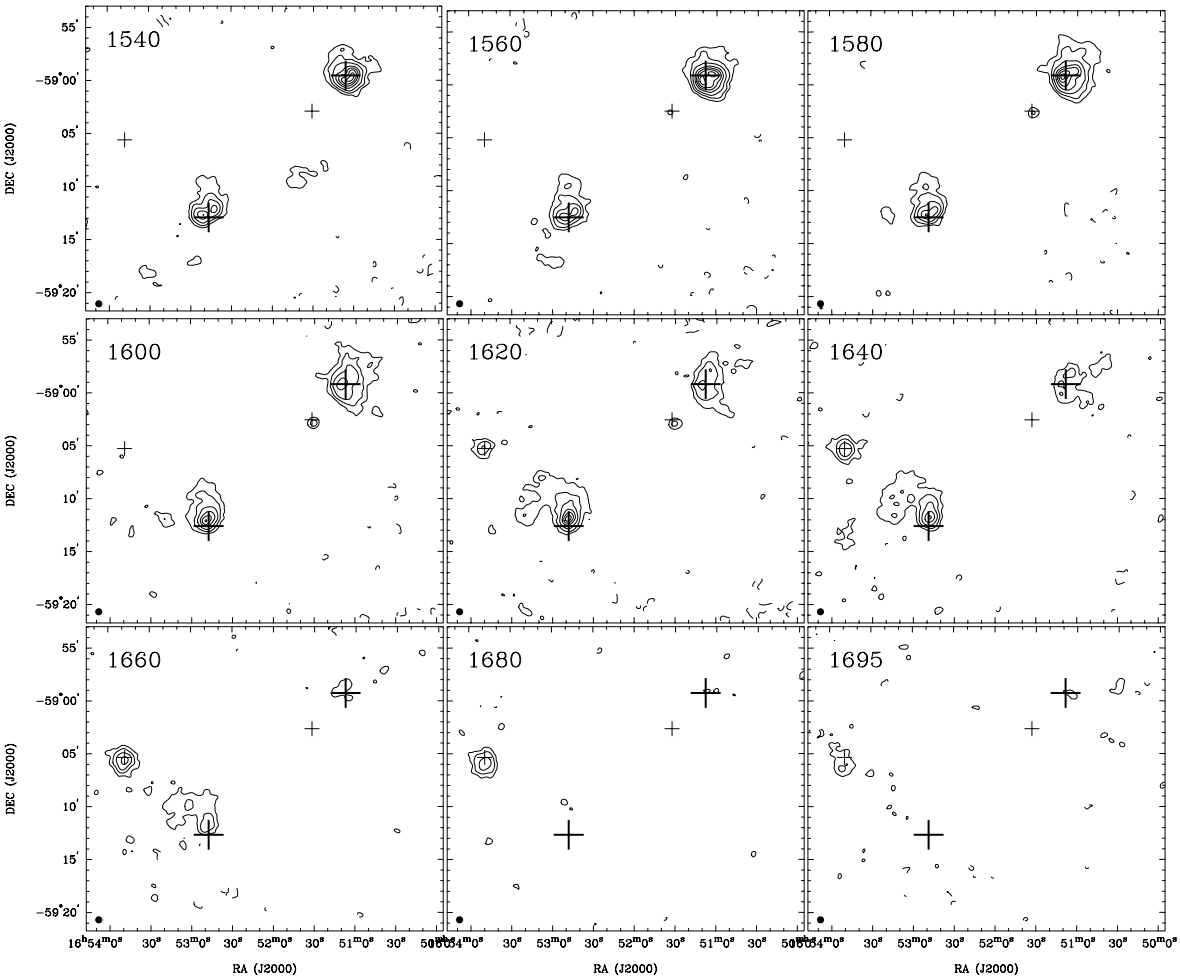

Figure 7 – *continued*

We measure an integrated H I flux density of $F_{\rm HI} = 67.5$ Jy km s^{-1} which corresponds to an H I mass of 5×10^9 M$_\odot$. About 80 per cent of the H I mass lies within the optical B_{25} radius (see Table 1).

Previous H I measurements, obtained with the 64-m Parkes telescope, include $F_{\rm HI} = 81 \pm 12$ Jy km s^{-1} (Whiteoak & Gardner 1977), 76.0 ± 5.7 Jy km s^{-1} (Reif et al. 1982), and 77.5 Jy km s^{-1} (Pence & Blackman 1984). From HIPASS we obtain $F_{\rm HI} = 91 \pm 7$ Jy km s^{-1} (see above), suggesting that ∼20 per cent of the H I emission in and around NGC 6221 resides in diffuse, extended H I clouds, not detected by the ATCA. For Dwarfs 1 and 2 which are located near NGC 6221 we measure integrated H I flux densities of 4.3 and 0.8 Jy km s^{-1}, respectively (see Table 3).

There are three H I extensions from the disc of NGC 6221 (see Fig. 10) that are kinematically distinct from the main disc. All three lie well to the east of the stellar disc. These are a 'plume' on the northern end of the galaxy that reaches from α, δ (J2000), $v_{\rm hel}$ = (16$^{\rm h}$52$^{\rm m}$51$^{\rm s}$, −59°09′45″, 1620 km s^{-1}) to (16$^{\rm h}$53$^{\rm m}$20$^{\rm s}$, −59°10′00″, 1660 km s^{-1}), a 'spur' which reaches to the east from (16$^{\rm h}$52$^{\rm m}$59$^{\rm s}$, −59°11′30″, 1460 km s^{-1}) to (16$^{\rm h}$53$^{\rm m}$22$^{\rm s}$, −59°11′54″, 1430 km s^{-1}), and a 'tail' that spreads out from the south end of the galaxy at (16$^{\rm h}$52$^{\rm m}$45$^{\rm s}$, −59° 16′ 00″, 1415 km s^{-1}), and curves back to (16$^{\rm h}$53$^{\rm m}$16$^{\rm s}$, −59°17′10″, 1385 km s^{-1}). The combined H I flux density of these extensions is ∼9 Jy km s^{-1}. The first and second moment maps on Fig. 10 clearly show the overlap between the spur and the plume in the area 16$^{\rm h}$53$^{\rm m}$05$^{\rm s}$ to 16$^{\rm h}$53$^{\rm m}$20$^{\rm s}$ and −59°11′ to −59°12′. The H I spectra show two features in this region, so that the second moment is unphysically large and the first moment appears discontinuous. The large value of the second moment in the spur does not indicate a deep potential well in this region, it reflects only the velocity separation of the two structures that overlap on the sky in this region, at 1460 and 1640 km s^{-1}.

The position–velocity diagram in the lower panel of Fig. 11 averages over the vertical axis of the upper panel; this can blend structures that are distinct spatially but overlap in projection. Some distinctions remain clear, however, like the gap between Dwarf 3 and the bridge at $x = 57$, where x is the projected scale ($x = 1^{\rm s} = 0.95$ kpc) along the x-axis as indicated in Fig. 11. The bridge is narrow in velocity, and it roughly follows a curve described by

$$v\,({\rm km\,s^{-1}}) = 1374 + 2.85x - 0.017x^2$$

with a width σ_v of only ∼20 km s^{-1} or less. Extending this curve to the east beyond NGC 6221 ($170 > x > 150$, $1380 < v < 1400$), we find it continues as the 'tail' described in the preceding paragraph (see also Fig. 10). We tentatively interpret this alignment on the position–velocity diagram to indicate a dynamical connection between the tail and the bridge; however, these velocities correspond to the range of rotation velocities of the disc of NGC 6221, which makes it plausible that this is a chance alignment of two unconnected structures.

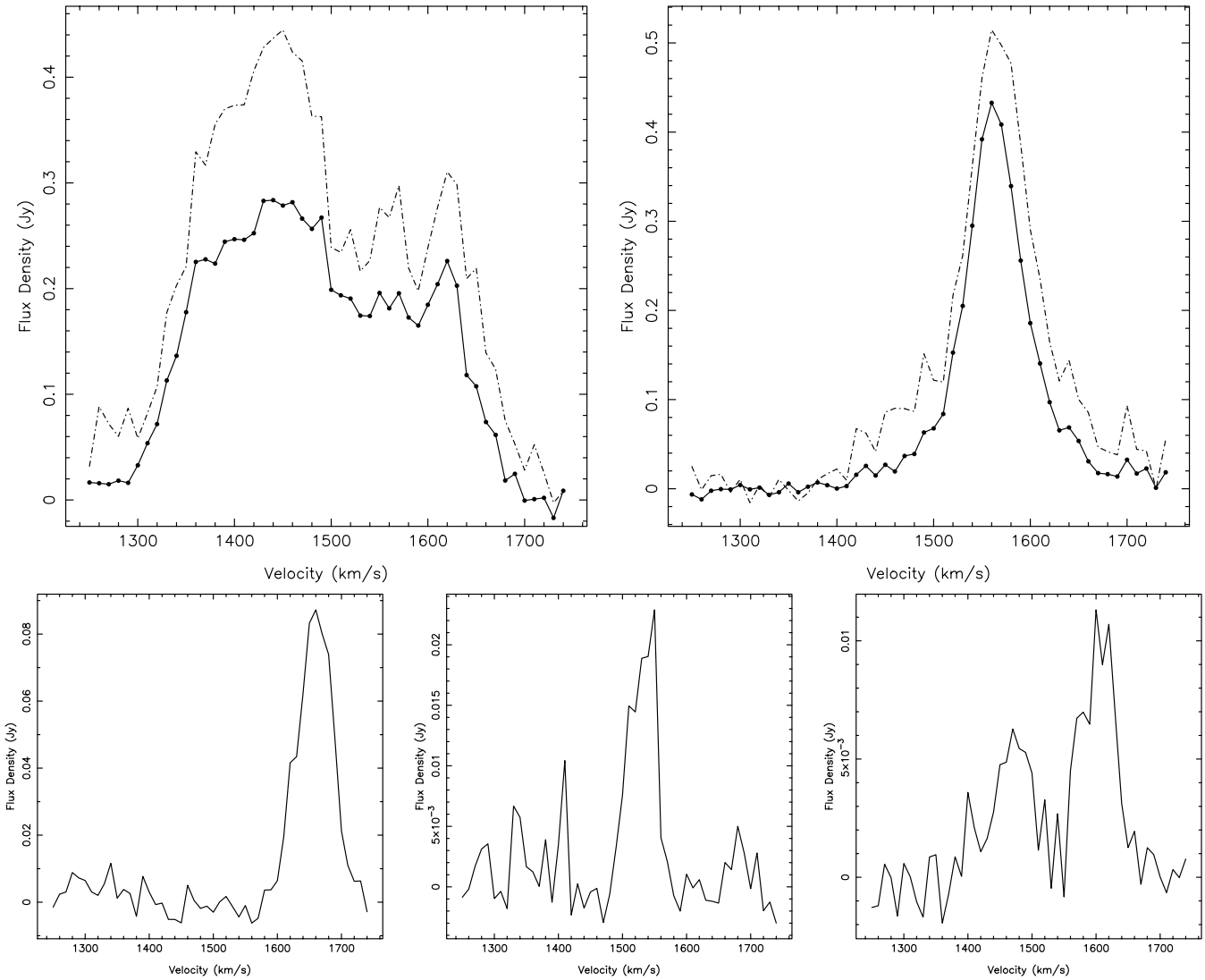

Figure 8. Top: H I spectra of NGC 6221 (left) and 6215 (right). The galaxy spectra were obtained over different areas, including (dotted lines) and excluding (solid lines) the irregular extensions. Bottom: H I spectra of the Dwarfs 1–3 (from left to right).

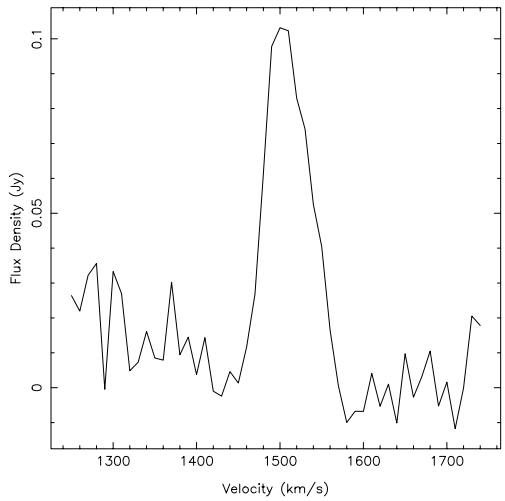

Figure 9. H I spectrum of the main bridge component.

While the plume, spur and tail extend predominantly to the east of the disc, the western side of NGC 6221 has a sharp edge in the H I map. Here the column density drops abruptly from $\sim 2 \times 10^{21}$ cm^{-2} to less than 5×10^{19} cm^{-2} over a distance of $\sim$4 kpc.

Further, we note that the HIPASS data show faint H I emission to the south ($\sim$1300 km s^{-1}) and east ($\sim$1400 km s^{-1}) of NGC 6221, outside the ATCA primary beam. This emission is potentially associated with additional dwarf galaxies in the group.

4.2 The galaxy NGC 6215

Fig. 12 shows the H I distribution of NGC 6215, the mean H I velocity field and the H I velocity dispersion. The H I distribution shows a depression in the central region, similar to that of NGC 6221, which is also illustrated in Fig. 13. The H I emission in NGC 6215 covers a velocity range from 1450 to 1660 km s^{-1}. We measure an integrated H I flux density of 35.2 Jy km s^{-1} which corresponds to an H I mass of 3×10^9 M$_\odot$. About 80 per cent of the H I mass lies within the optical B_{25} radius (see Table 1).

Reif et al. (1982) obtained a slightly larger value of $F_{\rm HI} = 39.7 \pm 4.4$ Jy km s^{-1} using the 64-m Parkes telescope. This contains a

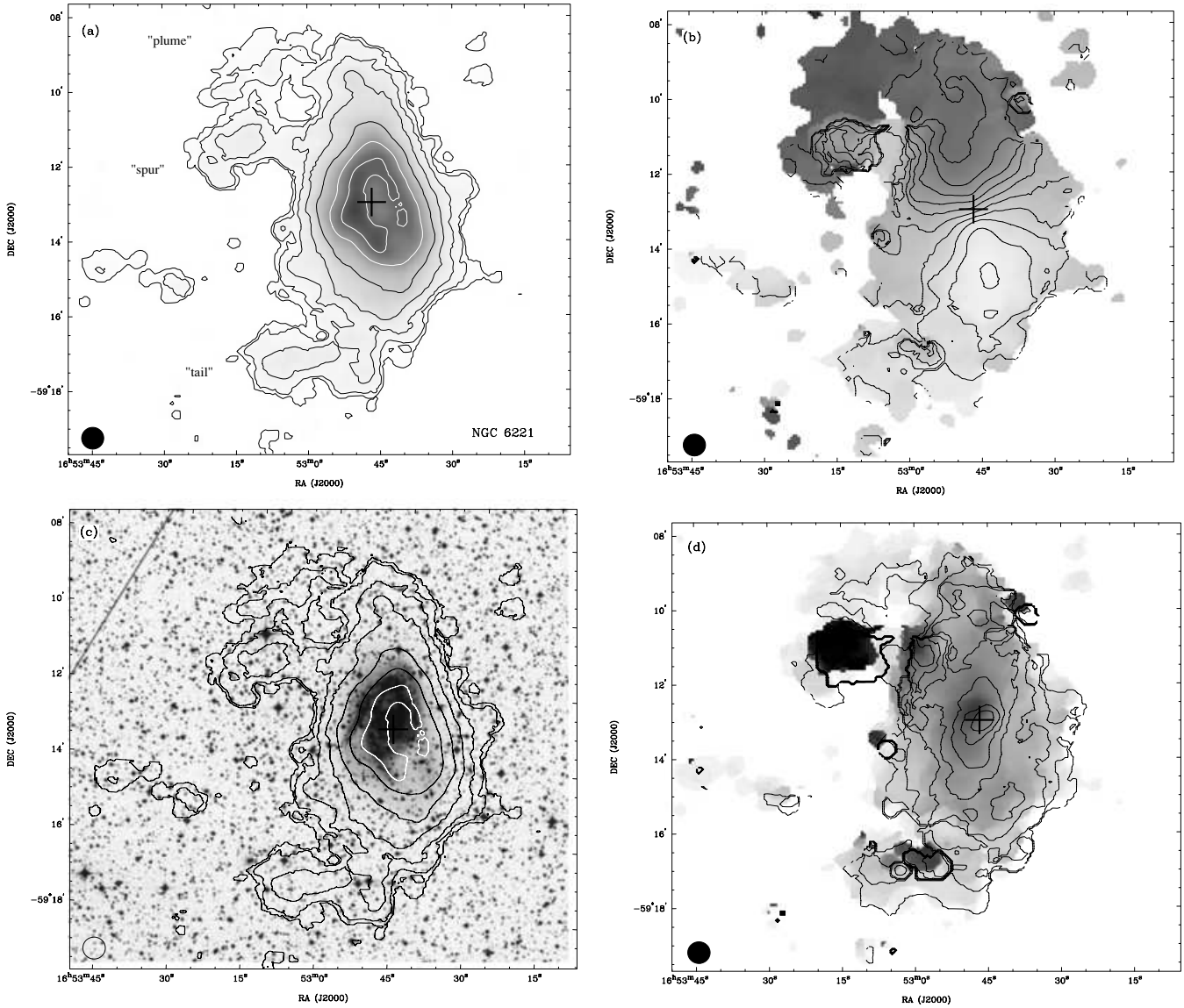

Figure 10. The barred starburst galaxy NGC 6221. (a) H I distribution (0. moment). The contour levels are 0.05, 0.1, 0.2, 0.4, 0.8, 1.6 and 2.4 Jy beam^{-1} km s^{-1} (corresponding to H I column densities of 4.6×10^{19} to 2.2×10^{21} atoms cm^{-2}). (b) Mean H I velocity field (1. moment). The contour levels range from 1375 to 1625 km s^{-1}, in steps of 25 km s^{-1}. The grey-scale ranges from 1350 (white) to 1800 km s^{-1} (black). (c) H I distribution (contours) overlaid on to a UKST *B*-band image (grey-scale) obtained from the SSS. The contour levels are as in (a). (d) H I velocity dispersion (2. moment). The contour levels are 10, 20, 30, 40, 50, 60 and 70 km s^{-1}. The grey-scale ranges from 0 (white) to 100 km s^{-1} (black). The synthesized beam (35 arcsec) is marked in the bottom-left corner, and the optical centre position (see Table 1) is marked with a cross.

small contribution from Dwarf 3 which has an integrated H I flux density of about 0.4 Jy km s^{-1} (1 per cent of NGC 6215), and some diffuse H I emission from the bridge. Using HIPASS we estimate $F_{\rm HI} = 57 \pm 7$ Jy km s^{-1} for NGC 6215 (see Section 4). This suggests that ~30 per cent of the H I flux density in and near NGC 6215 is in diffuse, extended gas that was filtered out by the interferometer.

In addition to its rotating disc, NGC 6215 shows an H I extension to the northeast which makes a hook shape in velocity (Fig. 12). It begins at α, δ (J2000), $v_{\rm hel} = (16^{\rm h}\,51^{\rm m}\,02^{\rm s}, -58^\circ\,56'\,30'', 1595\,{\rm km\,s^{-1}})$ and extends to $(16^{\rm h}51^{\rm m}11^{\rm s}.4, -58^\circ 55' 35'', 1585{\rm kms^{-1}})$. This 'hook' may be associated with the bridge between the two galaxies, as it seems to align with one end of the bridge. If so, its departure from the disc rotation pattern is probably a result of the interaction between NGC 6215 and 6221 in their recent encounter.

It is possible that the tail, spur, or plume features on the east side of NGC 6221, and the hook on the northwest of NGC 6215, may be tidal dwarf galaxies similar to those seen in the NGC 520 system (Hibbard & van Gorkom 1996; Delgado-Donate et al. 2003) and the M81 group (Makarova et al. 2002). It is difficult to determine whether they are gravitationally bound with the limited resolution and sensitivity of this study, but the question of whether we are seeing tidal dwarfs in formation is a fascinating topic for further study.

4.3 The dwarf galaxies

In addition to NGC 6221 and 6215, we detect three H I sources (see Fig. 6) which have faint optical counterparts. These are low-surface-brightness dwarf galaxies within the NGC 6221/15 group

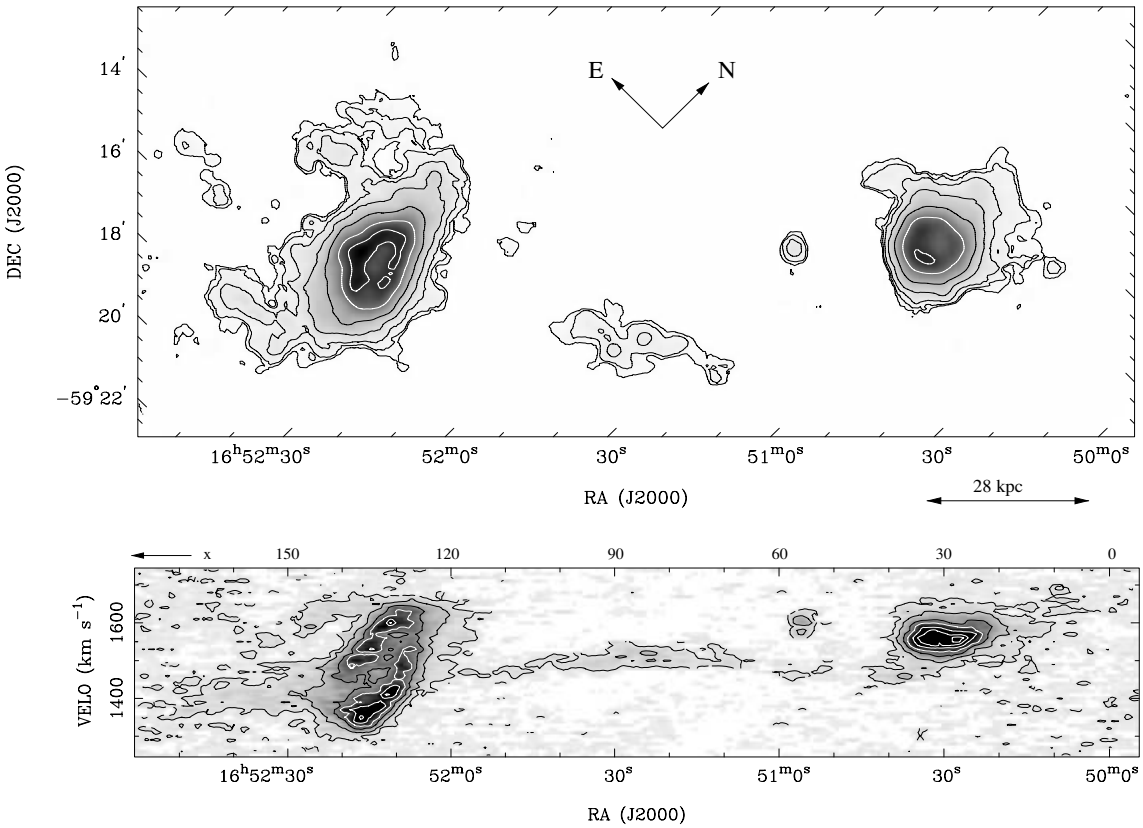

Figure 11. H I distribution in NGC 6221, 6215, Dwarf 3 and the bridge after rotation of the field by $-45°$. Top: H I distribution centred on the bridge area; the contour levels are 0.05, 0.1, 0.2, 0.4, 0.8, 1.6 and 2.4 Jy beam^{-1} km s^{-1} (as in Fig. 6). Bottom: H I position–velocity diagram of the same area. This panel was made by summing the rotated cube along the vertical axis in the upper panel. Note that the *x*-axes in the lower and upper panels are identical and show the projected right ascension. An interval of $1^{\rm m}$ on the *x*-axis corresponds to 10.8 arcmin or 56 kpc (see also the scale bar between the two panels). Before summing the H I flux over the *y*-axis, the data cube was blanked below 1.5 mJy beam^{-1} to decrease the noise contribution. The contour levels are 2, 3, 5, 7, 10, 13 and 16 mJy beam^{-1}. The bridge stands out as a long, thin, slightly curved filament connecting the interacting galaxies NGC 6221 and 6215.

and we refer to them as Dwarf 1, Dwarf 2 and Dwarf 3. The first two were previously also referred to as BK 1 and BK 2 (see Koribalski 1996a,b; Vega Beltrán et al. 1998) and were recently catalogued by Woudt & Kraan-Korteweg (2001). While Dwarf 1 (WKK 7689) and Dwarf 2 (WKK 7710) lie 11.1 arcmin northeast and 17.9 arcmin southeast of NGC 6221, respectively, Dwarf 3 lies only 4.4 arcmin east of NGC 6215 within the bridge area.

Dwarfs 1–3 have integrated H I flux densities of 4.3, 0.8 and 0.4 Jy km s^{-1} resulting in H I masses of 33, 6 and 3 $\times$ 10^7 $M_\odot$, respectively, (see also Table 3). Using Gaussian fits we obtain approximate major and minor axis diameters and PAs (deconvolved diameters are given in brackets): Dwarf 1, 72 $\times$ 54 arcsec^2 at *PA* = 175° (62 $\times$ 41 arcsec^2); Dwarf 2, 49 $\times$ 42 arcsec^2 at *PA* = 167° (34 $\times$ 23 arcsec^2); Dwarf 3, 43 $\times$ 35 arcsec^2 at *PA* = 229° (unresolved). We find that the fitted H I centre positions agree to within ~12 arcsec with the optical centre positions obtained from the SuperCOSMOS Sky Survey (SSS) images and those (see below) given by Woudt & Kraan-Korteweg (2001) and Kraan-Korteweg (private communication). The H I and optical properties of the three dwarf galaxies are summarized in Table 4.

Woudt & Kraan-Korteweg (2001) give the following optical properties.

(i) Dwarf 1 (WKK 7689): centre position α, δ(J2000) = $16^{\rm h}53^{\rm m}48^{\rm s}.7$, $-59°05'24''$, B_{25} magnitude = 15.2 mag, diameter = 74 $\times$ 42 arcsec^2 and extinction $A_{\rm B}$ = 0.583 mag. The H I velocity of 1559 $\pm$ 3 km s^{-1} (Huchtmeier, Karachentsev & Karachentseva 2001) quoted for this galaxy in the NASA/IPAC Extragalactic Database (NED) is incorrect. It originates from HIPASS data which have an angular resolution of 15.5 arcmin and include part of the northern, receding H I disc of NGC 6221 (see Fig. 6). From the ATCA data, we obtain a systemic velocity of 1655 km s^{-1} for Dwarf 1 (see Table 7).

(ii) Dwarf 2 (WKK 7710): centre position α, δ(J2000) = $16^{\rm h}54^{\rm m}29^{\rm s}.7$, $-59°25'13''$, B_{25} magnitude = 16.7 mag, diameter = 52 $\times$ 15 arcsec^2 and extinction $A_{\rm B}$ = 0.670 mag. It is an extended but very low-surface-brightness irregular galaxy of type Im (Kraan-Korteweg, private communication).

For Dwarf 3, Kraan-Korteweg (private communication) provided us with the following optical properties. It is an extremely low-surface-brightness galaxy, most likely of type Irr, and fairly face-on with a size of up to 20 $\times$ 15 arcsec^2, B_{25} magnitude $\approx$ 18.5 mag. The approximate centre position is α, δ(J2000) = $16^{\rm h}51^{\rm m}30^{\rm s}.6$, $-59°02'49''$.

The mean H I velocity fields of the three dwarf galaxies (see Fig. 14) show clear rotation patterns in the general area of the stellar counterparts, while outside that area the H I kinematics are less regular. In particular, the PAs of the stellar distributions roughly match those of the most regular part of the H I velocity fields. In Dwarf 1, the PA changes dramatically southeast of the optical area, possibly indicating a one-sided warp. Its velocity field shows some similarity to that of NGC 6215.

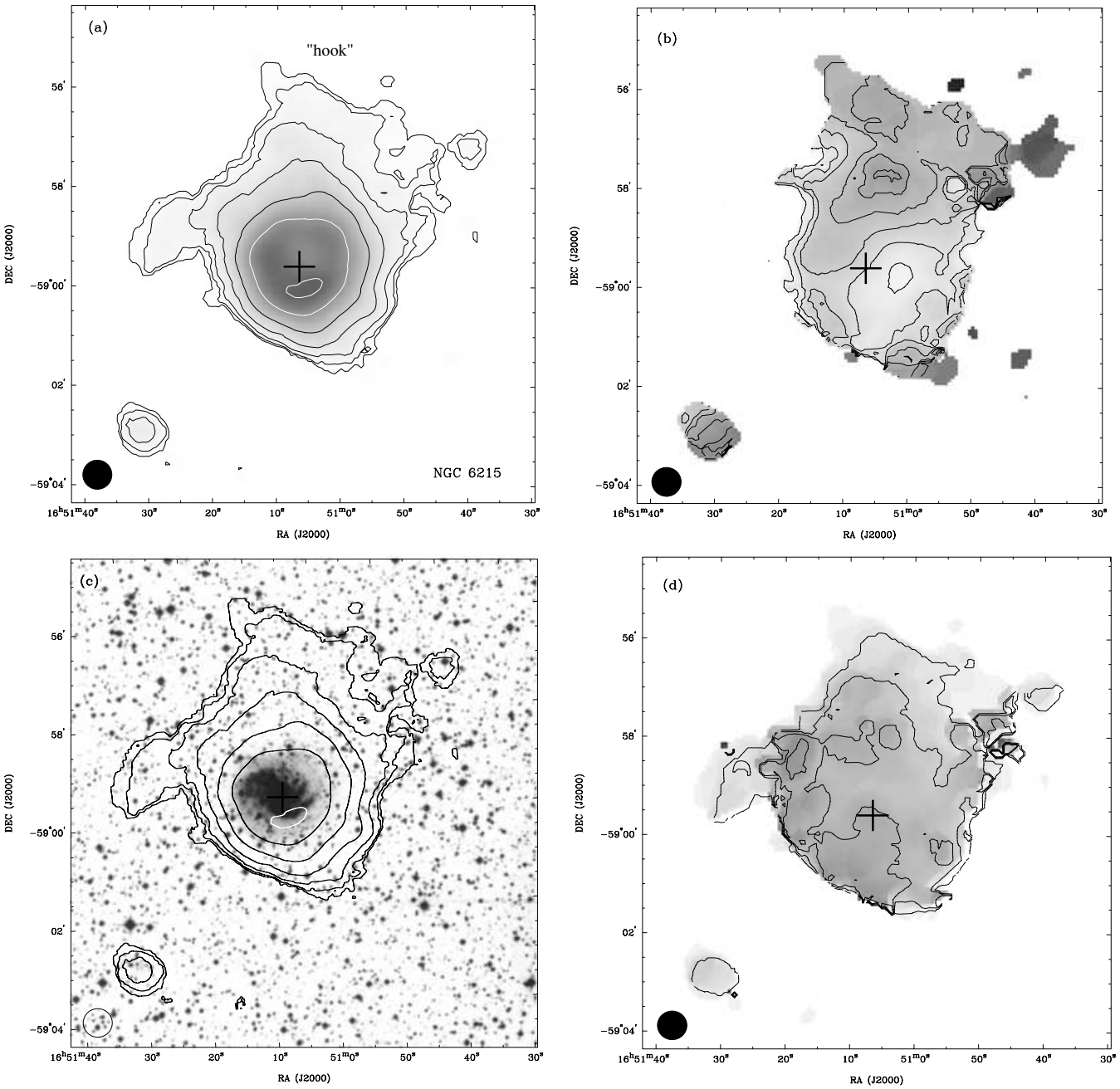

Figure 12. The galaxy NGC 6215 and Dwarf 3. (a) H I distribution (0. moment). The contour levels are 0.05, 0.1, 0.2, 0.4, 0.8, 1.6 and 2.4 Jy beam^{-1} km s^{-1} (corresponding to H I column densities of 4.6×10^{19} to 2.2×10^{21} atoms cm^{-2}). (b) Mean H I velocity field (1. moment). The contour levels range from 1550 to 1610 km s^{-1}, in steps of 10 km s^{-1}. The grey-scale ranges from 1540 (white) to 1700 km s^{-1} (black). (c) H I distribution (contours) overlaid on to a UKST *B*-band image (grey-scale) obtained from the SSS. The contour levels are as in (a). (d) H I velocity dispersion (2. moment). The contour levels are 10, 20, 30 and 40 km s^{-1}. The grey-scale ranges from 0 (white) to 100 km s^{-1} (black). The synthesized beam (35 arcsec) is marked in the bottom-left corner, and the optical centre position (see Table 1) is marked with a cross.

4.4 The H I bridge

Gaseous, intergalactic emission is detected between NGC 6221 and 6215 in the velocity range from ∼1460 to 1550 km s^{-1} (see Fig. 7). It commences at the western side of NGC 6221 and stretches nearly all the way to the southeast of NGC 6215 (see Fig. 11), extending over a projected distance of ∼100 kpc. The intergalactic gas appears to be concentrated in two streams (see Fig. 15) which create a wide, two-stranded bridge between the interacting galaxy pair NGC 6221/15. We measure an integrated H I flux density of 3.8 Jy km s^{-1} in the overall bridge area, corresponding to an H I mass of 3×10^8 M$_\odot$ (see Table 3). The brightest part of the H I bridge is located roughly mid-way between the two galaxies. No stellar counterpart to the bridge has been detected in the available optical sky surveys. The position–velocity diagram emphasizes the continuity of the H I bridge in velocity which we use to derive its age. The velocity gradient along the main (south-western) part of the bridge (length ∼7.3 arcmin or 38 kpc, see Fig. 11) is ∼8.3 ± 1.5 km s^{-1} arcmin^{-1} or ∼1.6 ± 0.3 km s^{-1} kpc^{-1}. The reciprocal value of the gradient gives a rough estimate for the time since the encounter of

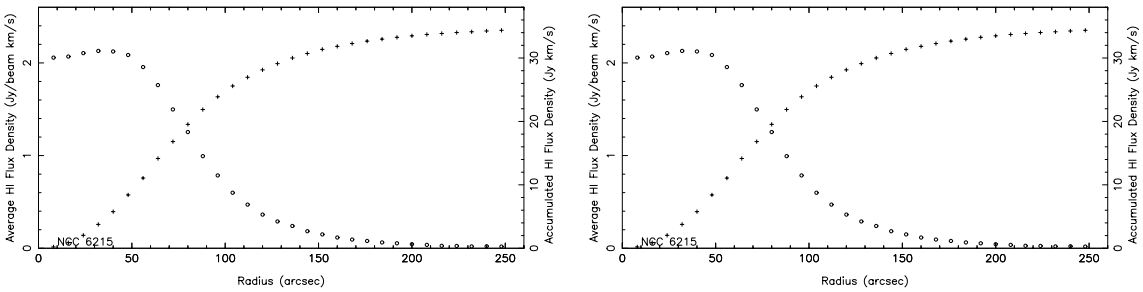

Figure 13. Radial H I distribution of the galaxies NGC 6221 (left) and 6215 (right).

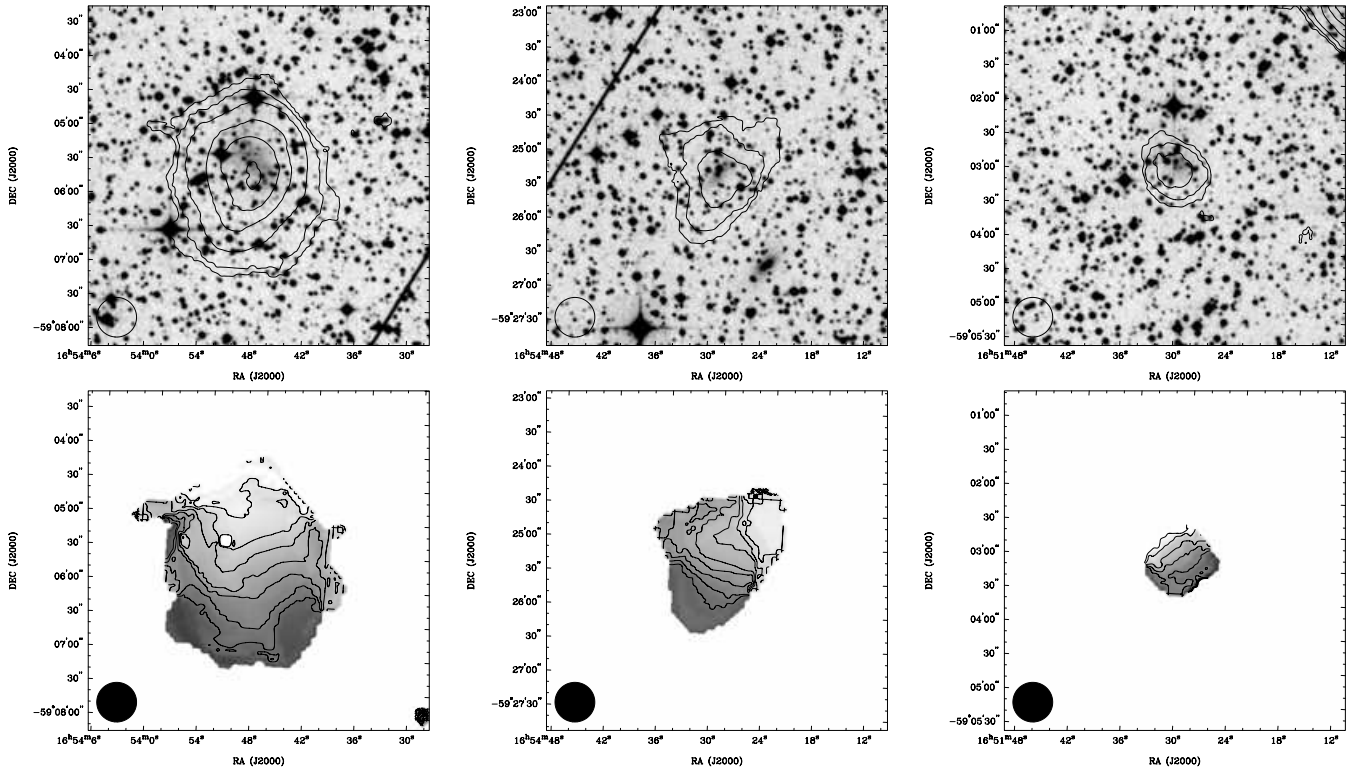

Figure 14. The three low-surface-brightness dwarf galaxies, Dwarfs 1–3 (from left to right). Top: H I distribution (contours) overlaid on to a UKST *B*-band image (grey-scale) obtained from the SSS. The contour levels are 0.05, 0.1, 0.2, 0.4, 0.6 and 0.8 Jy beam^{-1} km s^{-1} (corresponding to H I column densities of 4.6×10^{19} to 7.4×10^{20} atoms cm^{-2}). Bottom: Mean H I velocity field. The contour levels range from 1645 to 1675 km s^{-1} (Dwarf 1), 1510 to 1545 km s^{-1} (Dwarf 2), 1590 to 1610 km s^{-1} (Dwarf 3), all in steps of 5 km s^{-1}. The synthesized beam (35 arcsec) is marked in the bottom-left corner. Each field has a size of 5×5 arcmin^2.

$\sim 6 \times 10^8$ yr. This is an extremely long and old bridge. Because we measure only the radial velocity and the length of the bridge projected on a plane perpendicular to the radial direction, this estimate is obviously very rough. To do better would require knowledge of the three-dimensional trajectories of the two galaxies. Extrapolating the velocity gradient to the main galaxies and beyond shows that the tail on the southern end of NGC 6221, and possibly the north-western extension of NGC 6215, aligns very well with the velocity field of the bridge. We note that the steepest gradient of about 4–5 km s^{-1} kpc^{-1} is found within a 10-kpc region of the brightest part of the bridge.

There are three clumps in the main part of the bridge with $F_{\rm HI} =$ 0.39, 0.38 and 0.20 Jy km s^{-1} at α, δ(J2000) $= 16^{\rm h}51^{\rm m}41\overset{\rm s}{.}7$, $44\overset{\rm s}{.}6$ and $25\overset{\rm s}{.}1$, $-59^\circ 08' 41''$, $09' 38''$ and $07'\ 47''$, respectively, similar to the H I flux density observed in Dwarf 3 (0.35 Jy km s^{-1}, Table 3).

5 H I KINEMATICS

In this section we describe the kinematics of the various H I structures in the NGC 6221/15 group. For the galaxies, we fit rotation curves using the AIPS task ROCUR; the results are given in Tables 5–7. Several fits were performed for each object, fitting simultaneously different combinations of the parameters. First, we use a broad radial range to determine values of the global parameters: the systemic velocity ($v_{\rm sys}$) and kinematic centre position. Then we fit simultaneously, as functions of radius, the rotation velocity ($v_{\rm rot}$), inclination (i) and PA. There is little systematic variation in the inclination or PA with radius, so we fix them to their mean values, and refit the rotation velocity as a function of radius (see Tables 5 and 6) to obtain the rotation curves shown below (Fig. 16). Table 7 lists the fitted values of each of these parameters, as well as the maximum

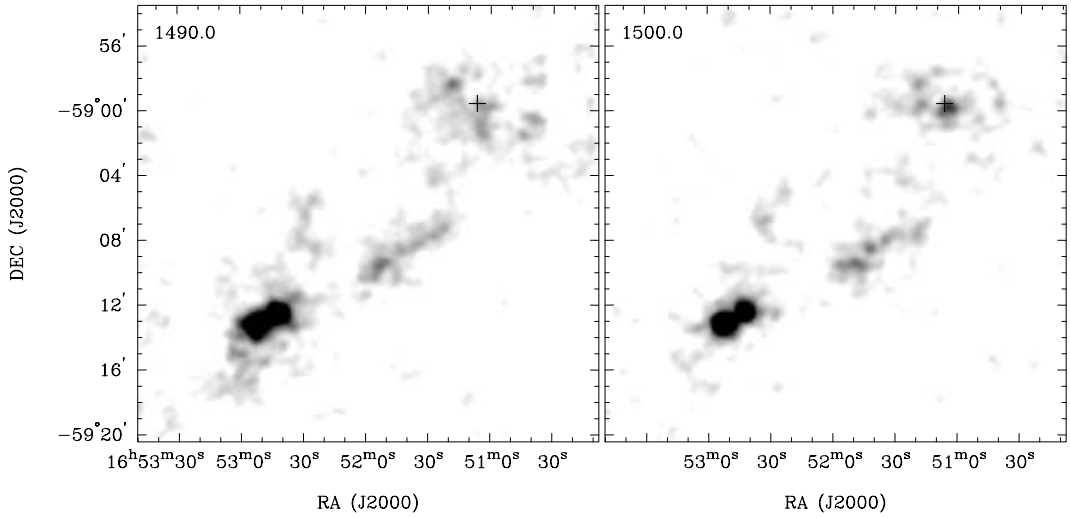

Figure 15. H I channel maps at velocities of 1490 and 1500 km s^{-1} to emphasize the wide two-stranded bridge between the interacting galaxies NGC 6221 and 6215.

value of the rotation velocity, $v_{\rm max}$, and the radius at the maximum rotation velocity, $r_{\rm max}$.

5.1 The galaxy NGC 6221

NGC 6221 is gravitationally the dominant system in the group. It shows a clear disc rotation pattern over the area of the optical galaxy, with several H I extensions beyond this area at different velocities. By fitting all parameters simultaneously for radii from 60 to 120 arcsec, we find the kinematic centre of NGC 6221 at α, δ(J2000) = $16^{\rm h}52^{\rm m}46\overset{\rm s}{.}14(\pm0\overset{\rm s}{.}3)$, $-59°12'55\overset{''}{.}8(\pm2'')$, a systemic velocity of $v_{\rm sys} = 1490 \pm 2$ km s^{-1}, a *PA* of $15° \pm 2°$, and an inclination angle of $i = 43 \pm 4°$. With these parameters fixed, we derive a rotation curve for NGC 6221 (Table 5) which is shown in Fig. 16, with the two sides, approaching (AS) and receding (RS), fitted separately and together (BS for 'both sides'). The rotation velocity rises to a maximum of about 170 km s^{-1} (deprojected) at radius of 105 arcsec (9 kpc). Beyond this, the rotation velocity decreases with radius, but not as fast as for a Keplerian potential. It reaches ∼140 km s^{-1} at a radius of 200 arcsec (17 kpc). These numbers indicate enclosed masses of 6×10^{10} M$_\odot$ inside 9 kpc and 8×10^{10} M$_\odot$ inside 17 kpc. For comparison, the virial mass (see Heisler, Tremaine & Bahcall 1985) of the NGC 6221/15 group is about 10^{12} M$_\odot$. The nominal errors in the rotation velocity are less than 1 km s^{-1} inside a radius of 150 arcsec, increasing to about 2 km s^{-1} at the largest radius. However, a better estimate of the error is from the difference between the fits on the two sides of the galaxy, which gives ±10 km s^{-1} or less over most of the disc. This translates to an error of about 15 per cent in the total mass estimate (at the adopted distance of 18 Mpc). Fig. 16 shows in dashed lines the enclosed mass, $M_<$, implied by the radius, r, and velocity, $v_{\rm rot}$, assuming circular rotation and spherical symmetry, i.e.

$$\frac{M_<}{\rm M_\odot} = 2.31 \times 10^5 \frac{r}{\rm kpc} \left(\frac{v}{\rm km\,s^{-1}}\right)^2 \qquad (1)$$

Table 5. Radial dependence of the rotational velocity, $v_{\rm rot}$, of NGC 6221. Using ROCUR the following parameters were fixed: $i = 43°$, $v_{\rm sys} = 1490$ km s^{-1} and $PA = 15°$. We list the fitting results for both sides (BS), the receding (northern) side (RS), and the approaching (southern) side (AS).

Radius (arcsec)	$v_{\rm rot}$ (km s^{-1}) (BS)	(RS)	(AS)
12.5	58.8 ± 2.9	61.9 ± 4.0	55.3 ± 4.11
27.5	107.3 ± 1.5	100.1 ± 1.6	114.8 ± 2.21
42.5	136.3 ± 1.1	127.6 ± 1.4	144.5 ± 0.87
57.5	152.2 ± 0.7	149.8 ± 1.1	154.5 ± 0.78
72.5	160.3 ± 0.4	162.0 ± 0.6	158.5 ± 0.54
87.5	166.2 ± 0.3	167.9 ± 0.4	164.6 ± 0.50
102.5	169.1 ± 0.4	167.9 ± 0.6	170.4 ± 0.57
117.5	168.0 ± 0.6	165.9 ± 1.1	170.2 ± 0.49
132.5	160.5 ± 1.1	153.6 ± 2.2	167.2 ± 0.41
147.5	155.0 ± 1.8	144.5 ± 3.5	165.3 ± 0.56
162.5	154.5 ± 2.3	149.1 ± 4.5	160.0 ± 0.82
177.5	152.2 ± 2.9	151.0 ± 5.8	153.3 ± 1.08
192.5	144.2 ± 3.0	151.8 ± 5.9	137.0 ± 1.43
207.5	138.7 ± 2.8	153.0 ± 4.9	121.7 ± 1.34
222.5	142.1 ± 2.3	158.0 ± 3.9	121.7 ± 1.51

Table 6. Radial dependence of the rotational velocity, $v_{\rm rot}$, of NGC 6215. Using ROCUR the following parameters were fixed: $i = 57°$, $v_{\rm sys} = 1572$ km s^{-1} and $PA = 11°$ (Model 1). We list the fitting results for both sides (BS), the receding (northern) side (RS), and the approaching (southern) side (AS). In addition, we list results obtained with $i = 45°$ (Model 2). In Model 3 we use the optical centre position, $i = 20°$, $v_{\rm sys} = 1561$ km s^{-1} and $PA = 50°$.

Radius (arcsec)	Model 1 ($i = 57°$) $v_{\rm rot}$ (km s^{-1}) (BS)	(RS)	(AS)	Model 2 ($i = 45°$) (BS)	Model 3 ($i = 20°$) (BS)
10	6.8	5.9	7.6	8.1	16.2
20	13.0	12.0	14.2	15.3	28.0
30	18.8	17.4	20.1	21.6	37.2
40	22.6	21.4	23.9	26.3	42.4
50	27.2	27.4	27.1	31.6	42.4
60	30.6	32.6	28.6	35.1	40.6
70	30.8	33.3	28.3	33.3	35.7
80	26.6	26.6	26.6	28.8	27.0
90	21.9	19.7	24.3	23.5	
$\sigma_{\rm vrot}$	±0.3	±0.5	±0.3	±0.4	±1.5

Table 7. Results from the rotation curve fitting of galaxies in the NGC 6221/15 group.

Object	Kinematic centre α, δ(J2000)	$v_{\rm sys}$ (km s^{-1})	i (degrees)	PA (degrees)	$v_{\rm max}$ (km s^{-1})	$R_{\rm max}$ (arcsec)	
NGC 6221	$16^{\rm h}52^{\rm m}46\overset{\rm s}{.}1$ ($\pm0\overset{\rm s}{.}3$), $-59^\circ12'55\overset{''}{.}8$ ($\pm2''$)	1490 ± 2	43 ± 4	15 ± 2	170 ± 10	105	
NGC 6215[a]	$16^{\rm h}51^{\rm m}02\overset{\rm s}{.}6$ ($\pm0\overset{\rm s}{.}6$), $-58^\circ58'45\overset{''}{.}0$ ($\pm5''$)	1572 ± 3	57	11 ± 2	31 ± 3	70	(Model1)
	$16^{\rm h}51^{\rm m}02\overset{\rm s}{.}6$ ($\pm0\overset{\rm s}{.}6$), $-58^\circ58'45\overset{''}{.}0$ ($\pm5''$)	1572 ± 3	45	11 ± 2	35 ± 3	70	(Model2)
	$16^{\rm h}51^{\rm m}06\overset{\rm s}{.}5$, $-58^\circ59'36''$ (opt. position)	1561 ± 3	20	50	41 ± 3	60	(Model3)
Dwarf 1	$16^{\rm h}53^{\rm m}48\overset{\rm s}{.}5$, $-59^\circ05'24''$ (opt. position)	1655	50	207	25 ± 5	90	
Dwarf 2	$16^{\rm h}54^{\rm m}29\overset{\rm s}{.}9$, $-59^\circ25'15''$ (opt. position)	1529	60	135	27 ± 3	70	
Dwarf 3	$16^{\rm h}51^{\rm m}31\overset{\rm s}{.}2$, $-59^\circ02'47''$ (opt. position)	1600	(40)	220	(31)		

[a]Note that it is likely that NGC 6215 is not in dynamical equilibrium.

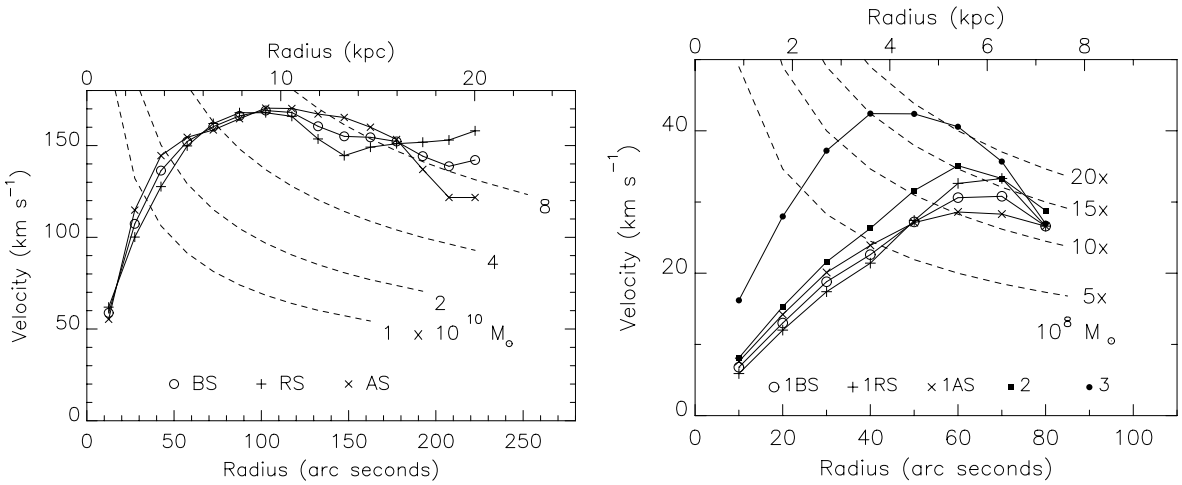

Figure 16. Rotation curve models for the two main galaxies, NGC 6221 (left) and 6215 (right). Dotted lines show the dynamical mass as a function of radius and rotation velocity. Note that the models for NGC 6215 are very uncertain as it is likely that the galaxy is not in dynamical equilibrium. For a description of the fit parameters and their uncertainties, see Section 5 and Table 7.

with values indicated in units of 10^{10} M$_\odot$. The last two radial points ($r > 18$ kpc) are poorly determined as the quality of the fit is decreasing in this region.

Using several long-slit Hα spectra, Pence & Blackman (1984) and Vega Beltrán et al. (1998) studied the kinematics of the ionized gas in the galaxy NGC 6221. The distribution of the ionized gas is mostly confined to the nuclear region, the bar ($r < 30$ arcsec) and H II regions along the spiral arms out to a radius of about 80 arcsec. The inner part of their major-axis rotation curve complements that derived from our mean H I velocity field.

The H I velocity field appears much more regular than the Hα velocity field (see Pence & Blackman 1984) which was reconstructed from several long-slit spectra. Recent Hα Fabry–Pérot observations of NGC 6221 (and NGC 6215) by Oddone et al. (1999) are expected to result in a more detailed velocity field of the ionized gas component in the inner region which can then be compared to that of the neutral gas.

5.2 The galaxy NGC 6215

The mean H I velocity field of NGC 6215 appears to show two rotation patterns (see Fig. 12). One pattern ($PA \sim 50^\circ$) is closely associated with the stellar distribution as well as the bulk of the H I gas. The other pattern ($PA \sim 10^\circ$) is significantly offset to the west of the optical galaxy but appears to reflect best the motions in the extended H I distribution. This ambiguity in the rotation patterns presents severe difficulties in finding the true rotation curve of NGC 6215. We also note that the H I velocity dispersion of NGC 6215 shows a pronounced gradient from the north-western part of the disc, where the lowest dispersion (~10 km s^{-1}) is measured, to the south-eastern part, where the dispersion reaches ~30 km s^{-1}. The location of the H I emission in the individual channel maps of NGC 6215 suggests that a substantial fraction of the gas (~1450–1510 km s^{-1}, ~1600–1650 km s^{-1}) may not be taking part in the disc rotation. The peculiar H I gas gives rise to the high-velocity dispersion in the eastern and south-eastern part of NGC 6215.

The fit parameters for the NGC 6215 disc, as given by ROCUR, using various approaches (described in detail below), are listed in Table 6. The rotation curves, $v(r)$, for each model are shown in Fig. 16.

With the PA of NGC 6215 fixed to 11° (±5°) we fit the remaining parameters simultaneously between radii from 45 to 90 arcsec and find the kinematic centre of NGC 6215 at α, δ(J2000) = $16^{\rm h}51^{\rm m}02\overset{\rm s}{.}6$ ($\pm0\overset{\rm s}{.}6$), $-58^\circ58'45\overset{''}{.}0$ ($\pm5''$), a systemic velocity of $v_{\rm sys}$ = 1572 ± 3 km s^{-1}. Note that in this fit the kinematic centre of NGC 6215 is offset by ~1 arcmin (5.2 kpc) from the optical centre position (see Table 1).

For comparison, Reif et al. (1982) derived a systemic velocity of $v_{\rm HI}$ = 1555 ± 7 km s^{-1} and a 20 per cent velocity width of w_{20} = 134 km s^{-1}. Using HIPASS, Koribalski et al. (2003) measured $v_{\rm HI}$ = 1564 ± 4 km s^{-1} and w_{20} = 149 ± 15 km s^{-1} for NGC 6215 (HIPASS J1651–58).

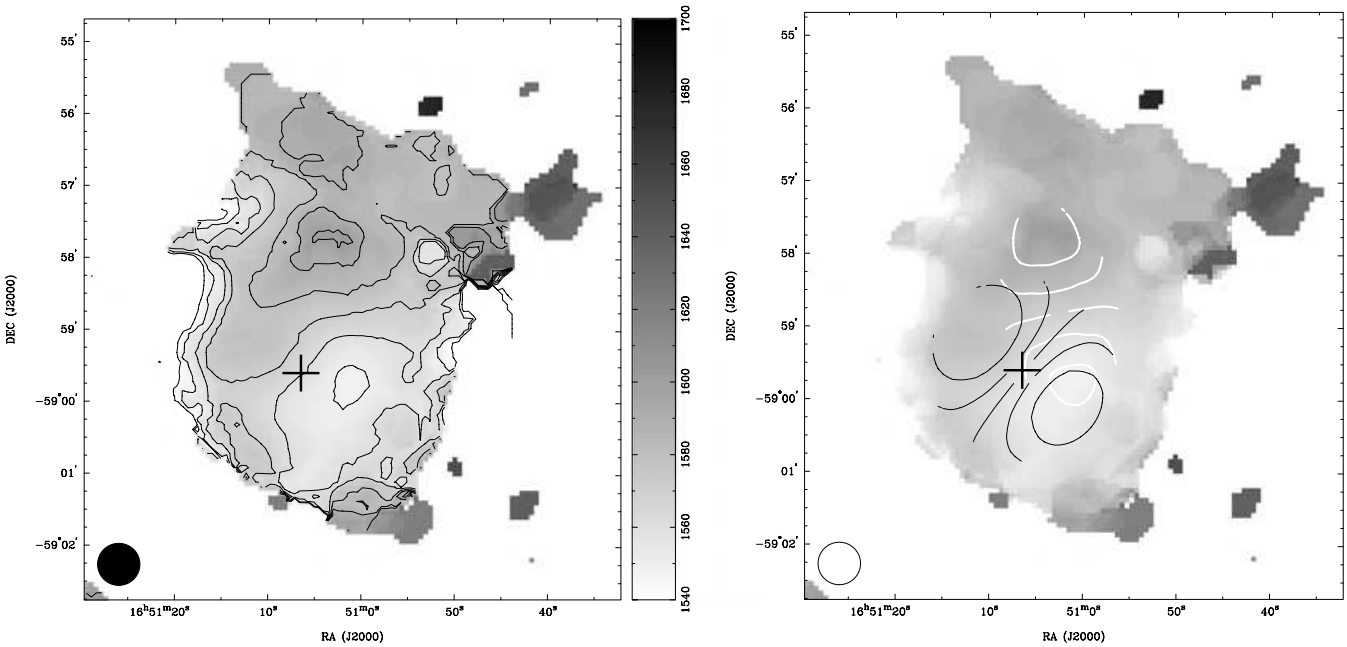

Figure 17. Observed and model velocity fields of the galaxy NGC 6215. (a) The observed, mean H I velocity field. The contour levels range from 1540 to 1600 km s^{-1} in steps of 10 km s^{-1}. (b) The observed, mean H I velocity field, displayed in grey-scale only, ranging from 1540 km s^{-1} (white) to 1700 km s^{-1} (black); see also Fig. 12(b). Overlaid are two very different velocity fields corresponding to Model 1 (in white, the contours range from 1550 to 1590 km s^{-1} in steps of 10 km s^{-1}) and Model 3 (in black, the contours range from 1550 to 1570 km s^{-1} in steps of 5 km s^{-1}). The synthesized beam (35 arcsec) is shown at the bottom-left corner, and the optical centre position (see Table 1) is marked with a cross.

For Model 1 we disregard the optical centre and use the north-western position as the centre of rotation to fit the velocity field. We obtain a well-behaved solution, showing a peak rotation velocity of ∼31 km s^{-1} at a radius of 60 to 65 arcsec (∼5.5 kpc). This is shown in Fig. 16 by the circles (for 'both sides'), + symbols (for the receding side, 1RS) and × symbols (for the approaching side, 1AS). The peak velocity depends on the inclination, which is not very well determined in the rotation curve fits. The nominal best-fitting inclination is 57°, but a fit with almost as good a result is obtained by forcing the inclination to a lower number. For Model 2 we choose an inclination of 45° and find a peak rotation velocity of ∼35 km s^{-1}, indicated by the filled squares in Fig. 16. Thus, the inclination has little impact on the result. Models 1 and 2 imply an enclosed dynamical mass, $M_<$, between 1.4 and 1.7 × 10^9 M$_\odot$ inside a radius of 70 arcsec (6.1 kpc). Beyond this radius the fit begins to fail, the resulting velocity for the receding side drops rapidly, which suggests that the velocity field in this region is not tracing circular rotation. The approaching side is well behaved out to about 8-kpc radius (90 arcsec), but with an enclosed mass estimate of only about 1.1 × 10^9 M$_\odot$. The problem with this model is that the optical galaxy, and most of the H I as well, are offset by some 5 kpc from the rotation centre.

If we set the centre of rotation to be the optical centre (see Table 1) and choose $PA = 50°$, $v_{\rm sys} = 1561$ km s^{-1} and $i = 20°$, we obtain a rotation curve with a peak rotation velocity of ∼41 km s^{-1} at a radius of 60 arcsec (5.2 kpc) resulting in a dynamical mass of ∼2 × 10^9 M$_\odot$. While the values for the PA and systemic velocity are reasonable in that part of the H I velocity field associated with the stellar distribution, the inclination of the galaxy remains difficult to determine. The H I emission of NGC 6215 in the channel maps shows large amounts of peculiar gas which appears not to participate in the disc rotation. The morphology of the bright H I emission in the velocity range from 1520 to 1590 km s^{-1} appears nearly circular, indicating a rather low inclination of the H I disc. We choose $i = 20°$ for the above fit but assign an error bar of 10° (resulting in $v_{\rm rot} = 28$–78 km s^{-1}) or more which makes the estimate of the dynamical mass very uncertain ($M_{\rm tot}$=1–8 × 10^9 M$_\odot$). The rotation curve given by this model (Model 3) is shown in Fig. 16 using filled circles; the model velocity field is shown in Fig. 17.

The dynamical masses resulting from these rotation curve fits are 1.4 × 10^9 M$_\odot$ inside 70 arcsec (6.1 kpc) for the offset centre (best fit, Model 1) case, and 2 × 10^9 M$_\odot$ inside 60 arcsec (5.2 kpc) for the fit where the centre position was set to the optical centre (Model 3). We note that all model rotation curves of NGC 6215 are falling at the largest radii.

The paradox of the NGC 6215 velocity field is that the gravitational mass indicated by the rotation curve fitting is less than the overall H I mass, and much less than the mass of the stars needed to explain the optical luminosity. If we restrict the mass comparison to the inner 60-arcsec radius around the optical centre position, we find $M_{\rm HI} = 10^9$ M$_\odot$ ($F_{\rm HI} = 14$ Jy km s^{-1}) and $M_{\rm tot} = 2 \times 10^9$ M$_\odot$ (assuming $i = 20°$), i.e. $M_{\rm HI}/M_{\rm tot} = 0.5$. The H I disc could have an even smaller inclination angle, e.g. $i = 10°$, which would boost the gravitational mass estimate to 7 × 10^9 M$_\odot$. A more likely explanation for the very weak rotation pattern is that the H I gas in NGC 6215 is not in dynamical equilibrium with the gravitational force, perhaps as a result of the encounter with NGC 6221. This would suggest that much of the gas will eventually collapse to the centre of the galaxy. Such a scenario is also consistent with the large amount of peculiar H I gas in NGC 6215.

5.3 The dwarf galaxies

In Fig. 14 we show the H I distribution and mean velocity field for each of the three low-surface-brightness dwarf galaxies. Using the H I velocity fields and, when necessary, optical properties of the

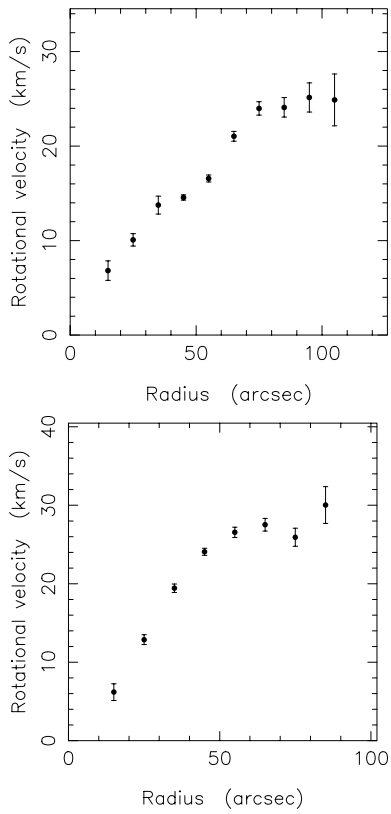

Figure 18. Rotation curve models for Dwarf 1 (top) and Dwarf 2 (bottom). The parameters are discussed in Section 5.3.

dwarfs, we try to characterize their rotation curves (using ROCUR) and derive their total dynamical masses. Due to some irregular velocity structures and the low angular resolution of the observations, compared to the size of the dwarf galaxies, it is rather difficult to achieve a consistent fit. A related factor may be the difference in centre position and extent of the H I compared to the stellar distributions (see Table 4). Consequently, the first difficulty we encounter is fitting the kinematic centre position of each galaxy (see also Section 5.2). As no consistent fit is achieved for either of the three dwarf galaxies, we use their optical centre positions instead. Further difficulties arise in fitting the position and inclination angles. We derive these iteratively by analysing the resulting model and residual H I velocity fields for numerous parameter combinations. A summary of the most reasonable parameters is given in Table 7 and the rotation curves are shown in Fig. 18.

We obtain a reasonable rotation curve for Dwarf 1 (WKK 7689) by using the optical centre position and setting $v_{\rm sys} = 1655$ km s^{-1}, $PA = 207^\circ$ and $i = 50^\circ$. Using these parameters we find a maximum rotational velocity of $v_{\rm max} = 25 \pm 5$ km s^{-1} (see Fig. 18) at a radius of ~90 arcsec (~8 kpc) resulting in a total dynamical mass of $\sim 11 \pm 4 \times 10^8$ M$_\odot$. For comparison, the H I mass is 3.3×10^8 M$_\odot$. Note that a substantial amount of the detected H I gas does not participate in the regular rotation described by the fitted rotation curve. The model and observed velocity fields differ most in the south-eastern part of the galaxy which shows rather different gas dynamics. We conclude that Dwarf 1 is strongly affected by the interactions in the NGC 6221/15 group.

For Dwarf 2 (WKK 7710) we obtain a reasonable rotation curve by setting $v_{\rm sys} = 1529$ km s^{-1}, $PA = 135^\circ$ and $i = 60^\circ$. Using these parameters we find a maximum rotation velocity of $v_{\rm max} = 27 \pm 3$ km s^{-1} at a radius of ~70 arcsec (~6 kpc) resulting in a total dynamical mass of $\sim 10 \pm 3 \times 10^8$ M$_\odot$. For comparison, the H I mass is 0.6×10^8 M$_\odot$. The irregular dynamics of a relatively small fraction of the H I gas appear to be confined to the north-eastern part of the galaxy.

For Dwarf 3, the smallest galaxy of the group, we find $v_{\rm sys} = 1600$ km s^{-1}, $PA = 220^\circ$. Because the galaxy is unresolved in our H I data, we cannot obtain a rotation curve. From the H I channel maps we estimate a rotation velocity of ~20 km s^{-1}, uncorrected for inclination. Assuming a maximum radius of ~15 arcsec we find that the total dynamical mass of Dwarf 3 is at least 1.2×10^8 M$_\odot$. The optical dimensions (see Table 4) indicate that the inclination is likely to be low; assuming $i = 40^\circ$ we find $M_{\rm tot} = 2.9 \times 10^8$ M$_\odot$. For comparison, the H I mass is only 0.3×10^8 M$_\odot$.

From the blue magnitudes of Dwarfs 1, 2 and 3 (Woudt & Kraan-Korteweg 2001; Kraan-Korteweg, private communication) we calculate luminosities of $L_{\rm B} \approx 4.0$, 1.1 and 0.2×10^8 L$_\odot$, and H I mass-to-light ratios of $M_{\rm HI}/L_{\rm B} = 0.83$, 0.55 and 1.5 M$_\odot$/L$_\odot$, respectively. All three dwarf galaxies appear to have rotational velocities around 20–30 km s^{-1}. While the gravitational masses for Dwarfs 1 and 2 are similar, ~10^9 M$_\odot$ (with uncertainties around 30–40 per cent), Dwarf 3 has a total mass of only ~0.3×10^9 M$_\odot$ (with even larger uncertainties). The resulting $M_{\rm tot}$ to $L_{\rm B}$ ratios are ~3, 9 and 15 M$_\odot$/L$_\odot$ (see also Table 8). Until higher-resolution multifrequency images (H I, CO, Hα) are available, these values should be regarded with caution.

6 DISCUSSION

For a full dynamical analysis of the NGC 6221/15 galaxy group, numerical simulations of the stars and the gas are needed. Here we will only give a qualitative picture of the interaction. The basic result of our H I observations is the presence of a wide, two-stranded gaseous bridge between NGC 6215 and 6221, the disruptions of their two discs, as well as three low-surface-brightness dwarf galaxies within the group.

Table 8. Mass and mass-to-light ratios of galaxies in the NGC 6221/15 group. Note that $M_{\rm HI}$, $M_{\rm tot}$ and $L_{\rm B}$ are measured out to different radii.

Object	$M_{\rm HI}$ (10^9 M$_\odot$)	$M_{\rm tot}$ (10^9 M$_\odot$)	$L_{\rm B}$ (10^9 L$_\odot$)	$M_{\rm HI}/L_{\rm B}$ (M$_\odot$/L$_\odot$)	$M_{\rm tot}/L_{\rm B}$ (M$_\odot$/L$_\odot$)	
NGC 6221	5.2	80	20.8	0.25	3.85	
NGC 6215	2.7	1.4	12.0	0.22	0.12	(Model 1, $i = 57^\circ$)
	2.7	1.7	12.0	0.22	0.14	(Model 2, $i = 45^\circ$)
	2.7	2.0	12.0	0.22	0.17	(Model 3, $i = 20^\circ$)
Dwarf 1	0.33	~1.1	0.40	0.83	~3	(WKK 7689)
Dwarf 2	0.06	~1.0	0.11	0.55	~9	(WKK 7710)
Dwarf 3	0.03	~0.3	0.02	1.50	~15	

6.1 The interaction

The H I bridge constitutes compelling evidence that the two galaxies have passed close to each other about half a billion years ago. The lack of a stellar counterpart to the bridge and its two prominent H I streams suggest this may be a 'collisional splash bridge' (Struck 1997, 1999). In this scenario the low-mass companion galaxy NGC 6215 may have plunged through the outer H I disc of the massive galaxy NGC 6221, splashing gas from both galaxies out into a wide two-stranded bridge. The bridge expands roughly along the path of the companion, which is now at a projected distance of ∼100 kpc from NGC 6221. The amount of H I gas detected in the bridge is 5 per cent (∼10 per cent) of that detected in NGC 6221 (NGC 6215). It could be even higher as diffuse extended H I emission, known to exist between the interacting galaxies, is filtered out by the interferometer (see Section 4). The gravitational pull from the individual galaxies gradually slows down the expansion of the ejected tidal debris (for a detailed discussion, see Hibbard & Mihos 1995). Material closest to either galaxy falls back fastest, while more distant debris return ever more slowly to accrete at larger distances from the galaxy centre. This may explain why the brightest parts of the H I bridge lie roughly mid-way between the two galaxies. The irregular H I extensions of both galaxies are likely to be the result of reaccretion over a long time-span. Because the galaxies would have rotated substantially during this period (∼1–2× for NGC 6221, and ∼0.5× for NGC 6215) ram pressure forces may also play a role in shaping the outer H I envelopes. In addition, it is possible that Dwarf 3 has formed out of bridge material (see, for example, Elmegreen, Kaufman & Thomasson 1993; Makarova et al. 2002; Delgado-Donate et al. 2003). Stellar population studies of this galaxy and the other galaxies are needed to get a handle on the evolution of the group.

The vigorous star formation in both galaxies, as well as the age spread of the stellar population in NGC 6221 (Cid Fernandes et al. 2003), indicates that reaccreted gas with low angular momentum may be falling into the nuclear region, triggering ongoing star formation and fuelling the active nucleus. While the inner disc of NGC 6221 looks rather undisturbed, apart from the peculiar shape of the optical arms, the low-mass companion appears severely affected by the collision. The H I distribution of NGC 6215 is rather asymmetric and its velocity field appears to show two rotation patterns. We have attempted to fit various rotation curve models, without satisfactory results, and conclude that NGC 6215 is most likely not in dynamical equilibrium. It is possible that H I gas reaccreted from the bridge is settling into a tilted plane offset from the old disc (Struck 1997).

6.2 Disc asymmetries and ram pressure

The H I distribution of the galaxy NGC 6215 (see Fig. 12) is clearly asymmetric. While the bright, south-eastern side of the disc (facing NGC 6221) appears compressed, the opposite side is fainter and extended. This asymmetry is also visible in the H I velocity dispersion which is two to three times higher on the compressed side, and the radio continuum emission which indicates enhanced star formation in that side. Apart from a weak extension to the east, the H I distribution of the spiral galaxy NGC 6215 is remarkably similar to that of the dwarf irregular galaxy Holmberg II (Ho II) which lies in the outskirts of the M81 group. Its comet-like appearance led Bureau & Carignan (2002) to suggest that Ho II is affected by ram pressure from an intragroup medium. Could ram pressure be a significant force in the NGC 6221/15 group in addition to the observed interactions? The H I velocity field of NGC 6215 is peculiar – the kinematical centre of the gas appears displaced by ∼5 kpc from the optical centre in the same direction as the pressure vector.

ASCA observations of NGC 6221 and its surroundings (see Levenson et al. 2001) show the hot X-ray emission to envelope all of the H I emission in NGC 6221. In addition, there is extended but very faint X-ray emission to the west of NGC 6221 (see Fig. 3), which may indicate the presence of hot intragroup gas. Higher sensitivity X-ray data as well as numerical simulations are needed to study the evolution of the gas and stars in the NGC 6221/15 group.

7 CONCLUSIONS

ATCA H I observations of the spiral galaxies NGC 6221 and 6215 reveal a complex interacting galaxy group with a total of five members and large amounts of intergalactic gas. Throughout the paper we assume a distance of 18 Mpc for the NGC 6221/15 group. In summary, we find the following.

(i) A wide, two-stranded H I bridge of at least 3×10^8 M$_\odot$, which can be traced between the interacting galaxies NGC 6221 and 6215 over a projected distance of 100 kpc. We measure a velocity gradient of $\sim 8.3 \pm 1.5$ km s^{-1} arcmin^{-1} or $\sim 1.6 \pm 0.3$ km s^{-1} kpc^{-1}, which gives a rough estimate for the time since the encounter of $\sim 6 \times 10^8$ yr. The long time-span would have allowed large amounts of bridge material to fall back on to the galaxies and resettle, which is consistent with the brightest part of the H I bridge lying halfway between the two galaxies.

(ii) Three low-surface-brightness dwarf galaxies (Dwarfs 1, 2 and 3) with H I masses of 3.3, 0.6 and 0.3×10^8 M$_\odot$ at distances of 11.1 arcmin (58 kpc), 17.9 arcmin (94 kpc) and 14.2 arcmin (74 kpc) from NGC 6221. We derive H I mass-to-light ratios of $M_{\rm HI}/L_{\rm B} =$ 0.83, 0.55 and 1.50 M$_\odot$/L$_\odot$, respectively. The total mass-to-light ratios of $M_{\rm tot}/L_{\rm B} \approx 3$, 9 and 15 M$_\odot$/L$_\odot$ should be regarded as preliminary until higher-resolution multifrequency (H I, CO, Hα) images are available. The smallest, previously uncatalogued galaxy, Dwarf 3, lies between NGC 6221 and 6215, and may have formed out of bridge material. It appears to have a relatively large amount of dark matter.

(iii) The barred spiral NGC 6221 appears to be gravitationally the dominant galaxy of the group. Its integrated H I flux density, as measured with the ATCA, is 67.5 Jy km s^{-1} (∼20 per cent lower than the HIPASS value) corresponding to $M_{\rm HI} = 5.2 \times 10^9$ M$_\odot$. Careful fitting of the rotating curve results in $v_{\rm rot} = 140$ km s^{-1} at $r = 17$ kpc, giving an enclosed mass of 8×10^{10} M$_\odot$. Its total blue luminosity is 2×10^{10} L$_\odot$ resulting in mass-to-light ratios of $M_{\rm HI}/L_{\rm B} = 0.25$ M$_\odot$/L$_\odot$ and $M_{\rm tot}/L_{\rm B} = 4$ M$_\odot$/L$_\odot$. We find peculiar optical 'arms' extending south, while irregular H I features, which start well outside the stellar distribution, extend to the east of NGC 6221. The irregular H I extensions are likely to be gas reaccreted out of the bridge.

(iv) Unusual H I kinematics in the companion NGC 6215, most likely resulting from a collision with the outer H I disc of NGC 6221. There are large amounts of peculiar gas, mainly outside its stellar distribution, which could be gas reaccreted out of the bridge. We note that the reaccreted gas may settle in a plane offset from the old disc. The H I distribution is asymmetric and could be described as a bow-shock morphology with a central depression. The integrated H I flux density of NGC 6215, as measured with the ATCA, is 35.2 Jy km s^{-1} (∼30 per cent lower than the HIPASS value) corresponding to $M_{\rm HI} =$ 2.7×10^9 M$_\odot$. Attempts to fit a rotation curve to the mean H I velocity field of NGC 6215 failed to give satisfactory results. If we

disregard the orientation of the stellar distribution, the fit results in a kinematic centre displaced ∼5 kpc to the east of the optical centre. It is likely that the H I gas in NGC 6215 is not in dynamical equilibrium with the gravitational force.

(v) A virial mass of $\sim 10^{12}$ $M_\odot$ for the NGC 6221/15 group which is a factor of 10 higher than the total dynamical mass of all group members together. The mean velocity of the group is 1569 km s^{-1} with a dispersion of 59 km s^{-1}. It is interesting to note that the most massive galaxy NGC 6221 has the most blueshifted velocity (v_{sys} = 1490 km s^{-1}) of the group.

(vi) The radio continuum emission of both spirals consists of a bright nucleus and diffuse circumnuclear emission extending as far as the optical disc, resulting in SFRs of 15 and 13 $M_\odot$ yr^{-1} for NGC 6221 and 6215, respectively. The collision of NGC 6215 with the outer disc of NGC 6221 is likely to have caused enhanced star formation in both galaxies. Later, reaccreted H I gas with low angular momentum may sink towards the nuclear region, causing ongoing star formation in both galaxies and providing fuel for the active nucleus of NGC 6221. For the dwarf galaxies, we derive SFR upper limits of 0.1 $M_\odot$ yr^{-1}.

The rich H I morphology in the NGC 6221/15 group, as revealed by our ATCA observations, indicates the potential for an enormous wealth of intergalactic/intragroup structures shedding light on the early evolution of an interacting system, as well as emphasizing the importance of the intragroup medium and the amount of dark matter in galaxies and galaxy groups.

ACKNOWLEDGMENTS

The observations were obtained with the Australia Telescope which is funded by the Commonwealth of Australia for operations as a National Facility managed by CSIRO. We thank Curtis Struck, Bruce Elmegreen, Jayanne English, Elias Brinks and Lister Staveley-Smith for many valuable comments on an earlier version of this paper. We also thank an anonymous referee for careful reading of the manuscript and numerous helpful suggestions. We are grateful to Renee Kraan-Korteweg for providing us with the optical properties of the dwarf galaxies in the group, particularly Dwarf 3. Also, we thank T. Lavezzi and J. Whiteoak for their help during the early stages of this project. Lavezzi was a US Fulbright Fellow at the Australia Telescope National Facility, CSIRO, during 1994–1995. We acknowledge use of HIPASS data, which were provided under the auspices of the Multibeam Survey Working Group. This research has made extensive use of the NED which is operated by the Jet Propulsion Laboratory, Caltech, under contract with the National Aeronautics and Space Administration. We acknowledge use of the SSS. The Digitized Sky Survey was produced by the Space Telescope Science Institute (STScI) and is based on photographic data from the UKST, the Royal Observatory Edinburgh, the UK Science and Engineering Research Council, and the Anglo-Australian Observatory. The deep *H*- and *B*-band images from Eskridge et al. (2002) were obtained through the NED.

REFERENCES

Aalto S., Booth R. S., Black J. H., Johansson L. E. B., 1995, A&A, 300, 369
Barnes D. G. et al., 2001, MNRAS, 322, 486
Boisson C., Durret F., 1986, A&A, 168, 32
Bonatto C., Pastoriza M. G., Alloin D., Bica E., 1998, A&A, 334, 439
Bressan A., Silva L., Granato G. L., 2002, A&A, 392, 377
Bureau M., Carignan C., 2002, AJ, 123, 1316
Buta R., 1995, ApJS, 96, 39
Cid Fernandes R., Leâo J. R. S., Lacerda R. R., 2003, MNRAS, 340, 29
Condon J. J., 1992, ARA&A, 30, 575
Delgado-Donate E. J., Muñoz-Tunñón C., Deeg H. J., Iglesias-Páramo J., 2003, A&A, 402, 921
de Vaucouleurs G., de Vaucouleurs A., Corwin H. G. Jr., Buta R. J., Paturel G., Fouqué P., 1991, Third Reference Catalogue of Bright Galaxies. Springer-Verlag, New York (RC3)
Di Nella H., Couch W. J., Parker Q. A., Paturel G., 1997, MNRAS, 287, 472
Durret F., Bergeron J., 1987, A&A, 173, 219
Elmegreen B. G., Kaufman M., Thomasson M., 1993, ApJ, 412, 90
Eskridge P. B. et al., 2002, ApJS, 143, 73
Haarsma D. B., Partridge R. B., Windhorst R. A., Richards E. A., 2000, ApJ, 544, 641
Harnett J. I., Loiseau N., Reuter H.-P., 1990, Rev. Mex. Astron. Astrophys., 21, 245
Heisler J., Tremaine S., Bahcall J. N., 1985, ApJ, 298, 8
Helou G., Soifer B. T., Rowan-Robinson M., 1985, ApJ, 298, L7
Hibbard J. E., Mihos J. C., 1995, AJ, 110, 140
Hibbard J. E., van Gorkom J. H., 1996, AJ, 111, 655
Huchtmeier W. K., Karachentsev I. D., Karachentseva V. E., 2001, A&A, 377, 801
Jarrett T. H., Chester T., Cutri R., Schneider S., Huchra J. P., 2003, AJ, 125, 525
Kennicutt R. C., 1998, ARA&A, 36, 189
Koribalski B., 1996a, in Buta R., Crocker D. A., Elmegreen B. G., eds, ASP Conf. Ser. Vol. 91, Barred Galaxies, IAU Coll. 117. Astron. Soc. Pac., San Francisco, 172
Koribalski B., 1996b, in Skillman E. D., ed., ASP Conf. Ser. Vol. 106, The Minnesota Lectures on Extragalactic Neutral Hydrogen. Astron. Soc. Pac., San Francisco, 238
Koribalski B. S. et al., 2003, AJ, submitted
Laustsen S., Madsen C., West R. M., 1987, Exploring the Southern Sky: A Pictorial Atlas from the European Southern Observatory. Springer-Verlag, Berlin
Levenson N. A., Cid Fernandes R., Weaver K. A., Heckman T. M., Storchi-Bergmann T., 2001, ApJ, 557, 54
Malkan M. A., Gorjian V., Tam R., 1998, ApJS, 117, 25
Makarova L. N. et al., 2002, A&A, 396, 473
Oddone M. A., Goldes G., Carranza G., Diaz R., Plana H., Boulesteix J., 1999, Bol. Asoc. Argentina Astron., 43, 71
Pence W. D., Blackman C. P., 1984, MNRAS, 207, 9
Reif K., Mebold U., Goss W. M., van Woerden H., Siegman B., 1982, A&A, 50, 451
Ryder S., Dopita M. A., 1993, ApJ, 88, 415
Ryder S., Buta R. J., Toledo H., Shukla H. Staveley-Smith L., Walsh W., 1996, ApJ, 460, 665
Sandage A., Bedke J., 1994, The Carnegie Atlas of Galaxies. Carnegie Institution, Washington, DC
Sanders D. B., Egami E., Lipari S., Mirabel I. F., Soifer B. T., 1995, AJ, 110, 1993
Storchi-Bergmann T., Calzetti, KinneyCalzetti D., Kinney A. L., 1994, ApJ, 429, 572
Strong A. W. et al., 1988, A&A, 207, 1
Struck C., 1997, ApJS, 113, 269
Struck C., 1999, Phys. Rep., 321, 1
Vega Beltrán J. C., Zeilinger W. W., Amico P., Schultheis M., Corsini E. M., Funes J. G., Beckman S. J. J., Bertola F., 1998, A&AS, 131, 105
Véron M. P., Véron P., Zuiderwijk E. J., 1981, A&A, 98, 34
Whiteoak J. B., Gardner F. F., 1977, Aust. J. Phys., 30, 187
Woudt P. A., Kraan-Korteweg R. C., 2001, A&A, 380, 441
Woudt P. A., Kraan-Korteweg R. C., Fairall A. P., 1999, A&A, 352, 39
Wray J. D., 1988, The Color Atlas of Galaxies. Cambridge Univ. Press, Cambridge

This paper has been typeset from a TEX/LATEX file prepared by the author.